



Unreported mass movements and future hazard in the Warwan basin, Jammu and Kashmir, Western Himalaya

Ashim Sattar¹, Shashi Kant Rai², Abhinav Alangadan¹, Adam Emmer^{3,4}, Sunil Dhar², Umesh Haritashya^{5,6}, Mohd. Farooq Azam⁷

¹*School of Earth, Ocean and Climate Sciences, Indian Institute of Technology Bhubaneswar, Odisha, India*

²*Department of Environmental Sciences, Central University of Jammu, Jammu and Kashmir, India*

³*Department of Physical Geography and Geoeiology, Faculty of Science, Charles University, Prague, Czechia*

⁴*Department of Geography and Regional Science, University of Graz, Graz, Austria (until 8/2025)*

⁵*Department of Earth and Environmental Geosciences, University of Dayton, Dayton, OH, USA*

⁶*Sustainability Program, University of Dayton, Dayton, OH, USA*

⁷*Indian Institute of Technology Indore, Madhya Pradesh, India*

Corresponding authors: Ashim Sattar and Adam Emmer

Email: ashim.sattar@gmail.com

adam.emmer@natur.cuni.cz



1 **Abstract:**

2 The Warwan sub-basin in Jammu and Kashmir is a remote glaciated region containing several
3 glacial lakes and has recently experienced population growth and infrastructure development.
4 Due to inaccessibility and geomorphic masking, multiple mass movement events including
5 avalanches and Glacial Lake Outburst Floods (GLOFs) have remained largely unreported. This
6 study analyzes three major avalanche events from the past two decades. The September 2005
7 and September 2020 avalanches originated from glaciers GL-B and GL-A within the same
8 glacier complex, while the March 2020 rock-ice avalanche initiated from the headwall of
9 glacier GL-F in an adjacent valley and terminated before reaching its ablation zone. Runout
10 mapping shows that the September 2020 avalanche descended from the headwall of GL-A and
11 impacted its proglacial lake, triggering a GLOF. In contrast, the September 2005 event
12 terminated before reaching the glacial lake that began forming in 1999 at the terminus of GL-
13 B. Geomorphic analysis indicates persistent sediment influx from meltwater streams of GL-D
14 and GL-E into the lake associated with GL-A, progressively infilling the basin. Continued
15 glacier retreat caused meltwater to accumulate behind the sediment infill, dividing the basin
16 into two disconnected lakes. Impact from the September 2020 avalanche led to complete
17 drainage of stored water and sediment, generating a downstream debris flow. Pre- and post-
18 GLOF imagery reveals breaching and widening of the outflow channel and deposition of a
19 debris fan downstream. The repeated history of mass movements and continued growth of
20 glacial lakes raise serious hazard concerns in the Warwan sub-basin. GLOF modeling identifies
21 Lake-B as potentially hazardous lake at the present condition posing significant downstream
22 risk. Settlements such as Youdu and Qaderna, along with bridges, roads, and residential
23 structures, lie within potential GLOF inundation zones. High sediment availability from past
24 mobilization and deposition along the valley increases the potential of debris flow cascades,
25 posing elevated risks to downstream infrastructure and hydropower, underscoring the need for
26 preparedness and mitigation planning. GLOF modeling suggest that early warning system
27 closer to the source will be able to provide a good lead time in case of potential GLOFs in the
28 valley.

29 **Keywords:** Glacial Lake; Avalanche; GLOF Cascade; Unreported GLOFs, Glacier retreat.

30

31



1 **1. Introduction:**

2 Since 2000, accelerated glacier ice loss driven by rising temperatures (Azam et al., 2018;
3 Bhattacharya et al., 2021; Bolch et al., 2012; King et al., 2019; Maurer et al., 2019) has been
4 observed, with lake-terminating glaciers showing substantially greater mass loss compared to
5 land-terminating glaciers (King et al., 2018; Pronk et al., 2021; Sato et al., 2022). This climate
6 change-induced retreat has transformed deglaciated regions into debris- and bedrock-
7 dominated landscapes, fostering glacial lake formation and expansion due to enhanced calving
8 and warm water-ice interactions (Carrivick and Tweed, 2013; Furian et al., 2022; King et al.,
9 2019; Nie et al., 2018; Rai et al., 2024; Sakai et al., 2000; Sattar et al., 2019; Watson et al.,
10 2020). Together, these complex and diverse glacier responses challenge accurate assessments
11 of future glacier dynamics and associated cascading hazards (Kargel et al., 2011; Pritchard,
12 2019; Wiltshire, 2014). Glacial lakes have notably increased in number (~53%), area (~51%),
13 and volume (~48%) globally in the last three decades (Shugar et al., 2020). With rapidly
14 increasing downstream population, agricultural activity, infrastructure, and hydroelectric
15 development, these expanding lakes pose increasing threats to communities and infrastructure
16 (Haeberli et al., 2017; Sattar et al., 2025a; Schwanghart et al., 2016).

17 The Hindu Kush Karakoram Himalaya (HKH) region experienced an increase in the number of
18 glacial lakes between 2500 and 5500 m elevation, with the most prominent rise observed
19 between 4000 and 4500 m (Ashraf et al., 2017). Specifically, lake numbers increased by ~24%
20 above 4000 m and ~32% below this elevation. However, not all glacial lakes can cause Glacial
21 Lake Outburst Floods (GLOFs), as their hazard potential depends on lake and moraine dam
22 characteristics and multiple triggering factors such as slope instabilities, possible permafrost
23 existence and degradation and extreme precipitation events, among others (Taylor et al., 2023;
24 Veh et al., 2025).

25 A GLOF event can release millions of cubic metres of water (Sattar et al., 2025a) and threatens
26 downstream infrastructure, settlements, and agricultural land, often resulting in significant loss
27 of life and livestock (Sattar et al., 2025b; J.-Y. Zhang et al., 2025; T. Zhang et al., 2023; Zheng
28 et al., 2021b). For instance, the October 2023 South Lhonak GLOF in Sikkim, India, resulted
29 in a severe disaster, claiming over 100 lives, inundating or damaging approximately 5,900
30 buildings and 31 major bridges, and affecting approximately 270 km² of agricultural land, and
31 completely destroyed the Teesta III hydropower dam located ~68 km downstream (Sattar et
32 al., 2025a; T. Zhang et al., 2025). This event also demonstrated the enormous sediment



1 mobilization typical of GLOFs, capable of altering landscapes far downstream. Interestingly,
2 there were recent GLOF events in the Himalaya that originated from small lakes but had
3 amplified impacts due to erosion dynamics. For instance, the 2016 Gongbatongsha GLOF
4 event in the Poiqu Basin of China (Sattar et al., 2022), which was amplified by the huge debris
5 eroded along the channel where the 2015 Gorkha earthquake deposited the majority of the
6 debris. The 2025 Limi Valley GLOF originated from the subglacial drainage of two small lakes
7 in the Nepal Himalaya (Sattar et al., 2025b). The village of Til was impacted, which shows
8 signs of bank erosion and collapse. The GLOF that occurred in the Mount Everest region in
9 August 2024 (Sherpa et al., 2025) impacted the Thame village, carrying suspended debris and
10 depositing it in the valley. Another disastrous event was the Kedarnath cascade, where rainfall,
11 GLOF, and debris flow cascaded and destroyed the Kedarnath settlement at Uttarakhand in
12 June 2013 (Allen et al., 2016).

13 All these events highlight the dominant role of debris transport, which depends on flow
14 dynamics, channel morphology, erosion, and the availability of loose sediment for
15 transportation. Water released during a GLOF event can efficiently erode and mobilize debris,
16 transforming floods into debris flows or hyperconcentrated flows (Sattar et al., 2025a). The
17 Himalaya recently experienced another devastating event that destroyed the Dharali settlement
18 in Uttarakhand (Kumar et al., 2025), where a multi-episodic debris flow descended through the
19 valley, depositing massive volumes of debris at the Bhagirathi River confluence.

20 Even though numerous GLOFs and mass movement have been reported globally and regionally
21 (Nie et al., 2018; Shrestha et al., 2023), many remain unreported due to remote locations, lack
22 of downstream community impact, and limited high-frequency satellite observations (Zheng et
23 al., 2021b). Veh et al. (2019) identified 22 previously unreported GLOFs that occurred after
24 the 1980s using Landsat imagery, while Zheng et al. (2021) found 176 new unreported GLOF
25 sources in the High Mountain Asia (HMA), ~95% moraine-dammed glacial lakes, of which
26 ~57% located in the Himalaya (Veh et al., 2019; Zheng et al., 2021a). Such unreported events
27 create significant gaps in regional GLOF inventories, leading to underestimated frequency-
28 magnitude relationships (Veh et al., 2022). Identifying these unreported past events is therefore
29 crucial for reconstructing geomorphic process regimes and understanding the hazard frequency
30 in mountain catchments (Carrivick and Tweed, 2013; Richardson and Reynolds, 2000; Veh et
31 al., 2025). These undocumented events offer critical insights into GLOF process chains,



1 sediment dynamics, and landscape evolution (Cook et al., 2018; Sattar et al., 2025a), enabling
2 improved hazard modeling and risk mitigation.

3 In the Union Territories of Jammu and Kashmir (J&K) and Ladakh, only a limited number of
4 destructive GLOFs have been documented (Ahmed et al., 2022; Majeed et al., 2021; Schmidt
5 et al., 2020). Mal et al. (2021) identified 4,418 glacial lakes and 636 transboundary lakes in the
6 Indian Himalayan region (IHR) and reported that J&K and Ladakh have the highest cumulative
7 degree of GLOF hazards (Mal et al., 2021). Additionally, Dubey and Goyal (2020) reported
8 J&K and Ladakh having the maximum number of glacial lakes that can potentially impact
9 downstream infrastructure (Dubey and Goyal, 2020). Historical examples include a 1971
10 GLOF 18 km upstream of Nymmo village that killed 16 people (Ikeda et al., 2016a), and a
11 2003 GLOF affecting Domkhar village, which destroyed bridges, water mills, and agricultural
12 land (Ikeda et al., 2016b). More recently, the 2014 Gya Glacier GLOF damaged agricultural
13 land and other infrastructures in Gya village (Majeed et al., 2021; Schmidt et al., 2020).

14 While most Himalayan GLOF research focuses on predictive modeling, reconstruction studies
15 remain scarce, despite their importance for understanding multi-step process chains capable of
16 triggering GLOFs. Reconstructing GLOF cascades also improves parametrization for
17 hydrodynamic models. For instance, the reconstruction of the South Lhonak GLOF has
18 highlighted how unstable lateral moraines can initiate a sequence of moraine failure,
19 displacement waves generation, overtopping, moraine erosion, and downstream flooding
20 (Sattar et al., 2025a).

21 This study is motivated by the limited research on unreported GLOFs, avalanches, and other
22 mass movements in the Himalayan region. Here, we report and reconstruct past avalanches and
23 GLOF and evaluate future GLOF hazard in a peri-glacial complex. Changes in glacier and lake
24 morphology are evaluated using multi-sensor data to understand the chain of events that act as
25 conditioning and triggering factors for GLOF hazard. Here, we analyze lake evolution,
26 expansion, sediment infilling, permafrost distribution, and avalanche-GLOF mechanisms in a
27 glacier-lake complex in the Western Himalaya. The specific objectives of the study include
28 modeling past mass movements and also quantifying future downstream GLOF exposure in
29 the Warwan sub-basin of J&K. Our findings provide a foundation for future GLOF research
30 and offer critical information for downstream infrastructure and land-use planning towards
31 building hazard-resilient mountain communities.

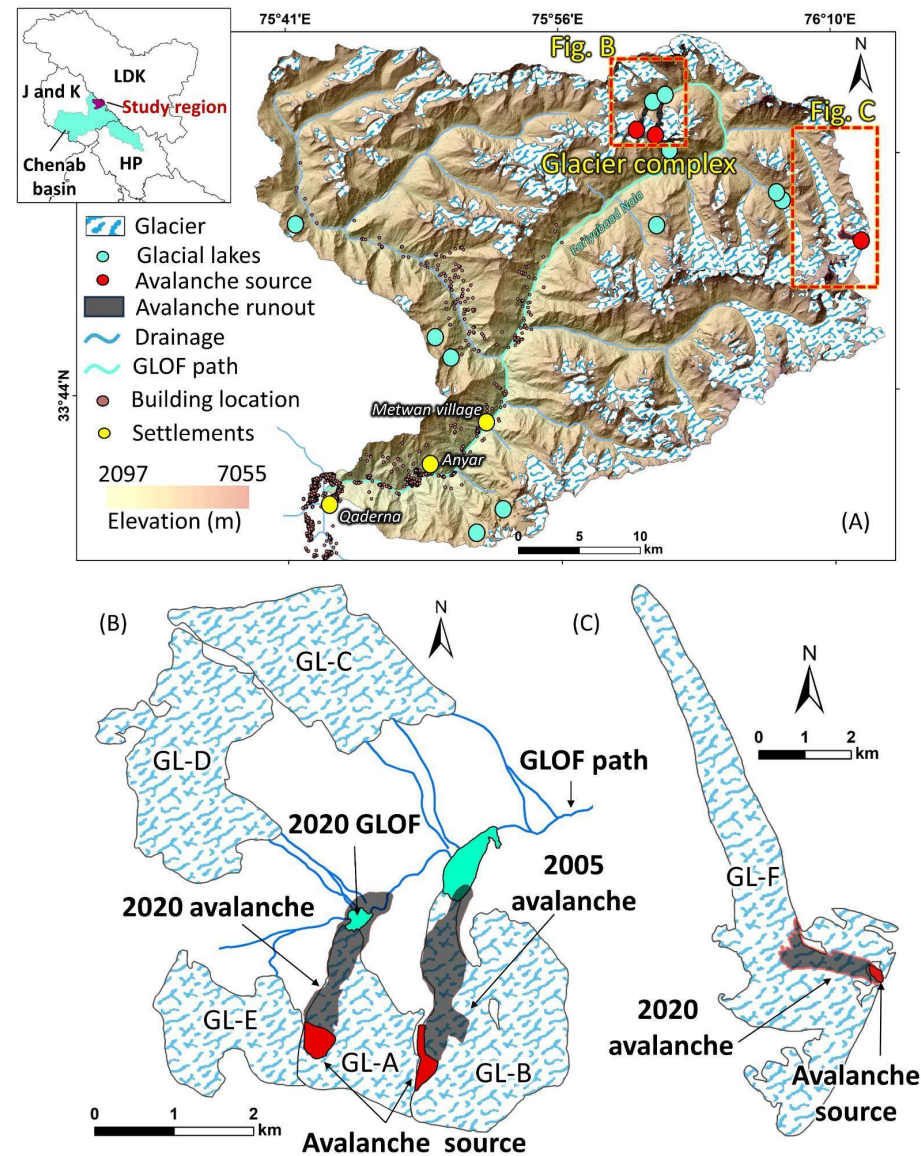


1 **2. Study area and importance of the region:**

2 The study area is situated in the Fariabad watershed within the Warwan sub-basin of the
3 Chenab River, located in the Kishtwar Himalaya of J&K, India (Fig. 1). The watershed
4 catchment covers an area of 1,403.8 km², with an average elevation of 4,308 m above sea level.
5 It contains 272 glaciers with a glaciated area of 314.61 km² (Pfeffer et al., 2014). This study
6 focuses on a glacier complex comprising 5 glaciers (GL-A to GL-E) (Fig. 1a) and an adjacent
7 glacier (GL-F) located opposite the glacier complex (Fig. 1c). The individual glacier area for
8 GL-A to GL-F are 2.2±0.014 km², 4.23 ±0.022 km², 3.49 ±0.02 km², 3.47±0.025 km², 2.16
9 ±0.016 km², 20.5±1.22 km², respectively (Pfeffer et al., 2014). In the glacier complex, GL-A
10 and GL-B are associated with proglacial lakes (named as Lake-A and Lake-B respectively) and
11 have experienced mass movement events in September 2020 and 2005, respectively. The
12 meltwater stream originating from this glacier complex forms the Fariabad Nalla, which
13 merges into the Marusudar River near Yordu village. Further, Marusudar flows southwards,
14 meeting the Chenab River near Bandarkoot. In the Fariabad watershed, the number of glacial
15 lakes has increased to twelve, rising from seven lakes in 1990 (G. Zhang et al., 2023). Most of
16 the glacial lakes in the watershed are isolated and not connected to any glacier. According to
17 Shean et al. (2020), the average elevation change (2000-2018) across all glaciers in the
18 catchment was $-0.33 \pm 0.28 \text{ m a}^{-1}$, with a mean mass balance of $-0.28 \pm 0.24 \text{ m we a}^{-1}$ (Shean
19 et al., 2020)

20 The nearby settlements (viz Qaderna, Yurod, Anyar, Rinaie, and Metwan) are located ~50-55
21 km downstream from the glacier complex, while major infrastructure such as the Bursar (800
22 MW) and Pakal Dul (1000 MW) hydropower sites are situated ~90 km downstream.
23 Additionally, several new settlements and agricultural activities have emerged along the
24 riverbank over the past two decades, as identified through high-resolution imagery from
25 Google Earth. Geologically, the region is seismically active with many past earthquakes,
26 clustered in the vicinity of the Kishtwar Window (Pandey et al., 2017).

27



1
2
3 **Fig. 1.** (A) The Warwan sub-basin, in the Chenab Basin of Jammu and Kashmir, showing the
4 distribution of the glaciers, glacial lakes, major settlements, previous avalanche source,
5 modeled GLOF path (also see Figure 10), and individual buildings; (B) glacier complex (GL-
6 A to GL-E) showing the locations of the 2020 avalanche-triggered GLOF and the 2005
7 avalanche; (C) glacier showing the 2020 avalanche from the headwall of the glacier.
8
9



1 **3. Data and methods:**

2 **3.1 Mapping glaciers, glacial lakes, and related processes**

3 The evolution of glaciers and associated glacial lakes was investigated using cloud- and snow-
4 free Landsat 7 and 8 imageries from 1999 to 2015 and PlanetScope imagery from 2016 to 2024
5 (Table S1). These images, captured predominantly during post-monsoon and peak ablation
6 periods, facilitated the delineation of glacier and glacial lake boundaries, as well as the mapping
7 of various geomorphic features and previous mass movement events including past avalanches
8 and GLOFs. Normalized Differential Water Index (NDWI) and standard FCC were used to
9 map the glacial lakes and glacier boundaries respectively (Rai et al., 2024). Glacier boundaries
10 were further refined through cross-validation with high-resolution imageries from Google
11 Earth and the Randolph Glacier Inventory (RGI) Version 6.0 (Pfeffer et al., 2014). PlanetScope
12 imagery was specifically used to detect past GLOFs, crevasses, ice calving, avalanche release
13 areas, and avalanche runouts. Associated geomorphic changes from these events were
14 documented using post-event PlanetScope imagery. Mapping uncertainty was calculated using
15 a half-pixel buffer, while lake area uncertainty was estimated using a full-pixel buffer
16 (Granshaw and Fountain, 2006; Racoviteanu et al., 2015).

17

18 **3.2. Avalanche reconstruction**

19 To reconstruct past avalanche events, we used the Rapid Mass Movement Simulation
20 (RAMMS) model, a well-established numerical tool designed for mass movement hazard
21 simulation. RAMMS operates based on the Voellmy-Salm rheological model, a finite volume
22 method that solves two-dimensional depth-averaged mass flow equations for avalanche-like
23 phenomena (Christen et al., 2010). This model accounts for complex interactions between the
24 avalanche material and terrain, making it highly suitable for alpine and glaciated environments
25 (Abhinav and Sattar, 2025; Sattar et al., 2022, 2021). The dynamics of avalanche flow within
26 RAMMS are governed by several key input parameters: the release area, release depth, material
27 density, friction parameters, and the terrain over which it flows. The release areas were
28 identified by detecting changes from pre- and post-event PlanetScope imagery. ALOS
29 PALSAR DEM (resampled to 12.5 m spatial resolution) was used to represent terrain for the
30 reconstruction.



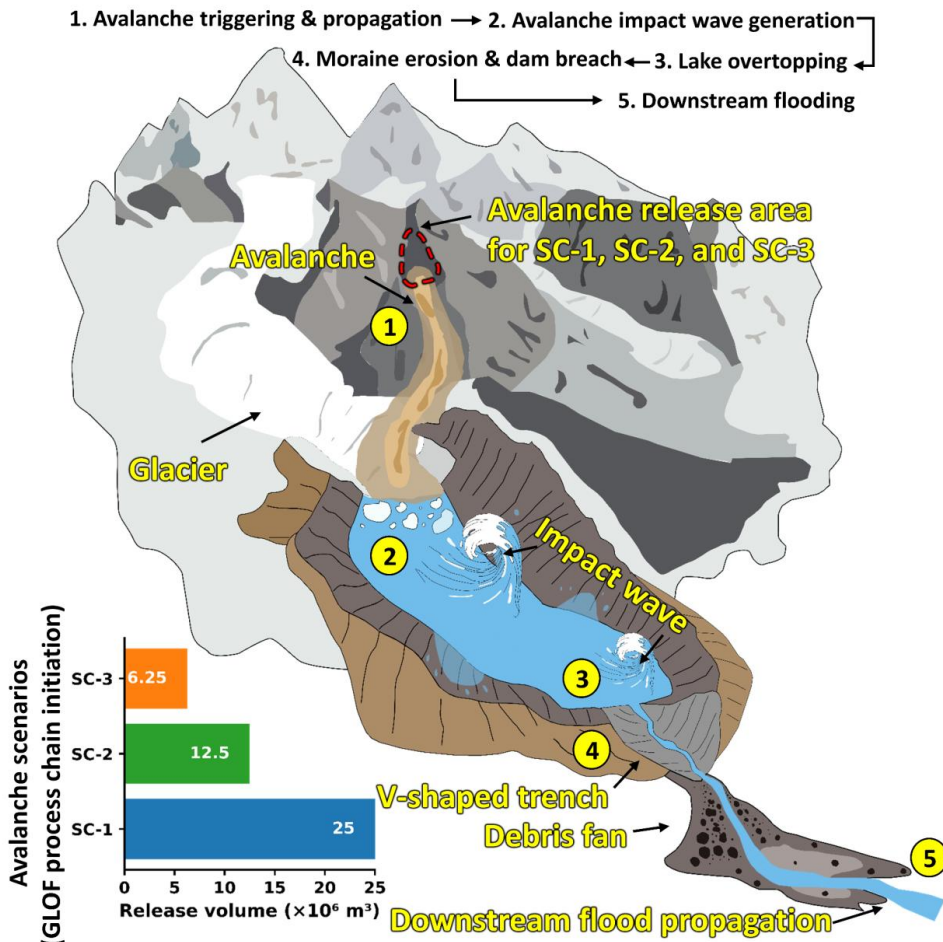
1 To accurately represent avalanche initiation, we conducted simulations with variable release
2 depths/volumes, adjusting these iteratively until modeled runouts matched observed avalanche
3 runouts. Scenario-based modeling initiated with a smaller release volume (R1) and
4 progressively increased volumes (R2-R4) to evaluate the influence of flow magnitude on
5 runout behavior. The material density (ρ) was assumed to be 1000 kg m^{-3} , reflecting a mixed
6 composition of snow, debris, and meltwater, consistent with previous avalanche modeling
7 studies (Sattar et al., 2021). The rheological behavior of the avalanche material in RAMMS is
8 controlled by two friction parameters: Coulomb-type basal friction (μ), representing basal
9 sliding resistance, and Turbulent friction (ζ), representing velocity-dependent resistance due to
10 internal turbulence. We set $\mu = 0.12$ and $\zeta = 1000 \text{ m s}^{-2}$, values widely adopted in high-
11 mountain avalanche and debri-flow simulations (Frey et al., 2018; Sattar et al., 2022; Schneider
12 et al., 2014; Somos-Valenzuela et al., 2016). The RAMMS outputs provide spatially distributed
13 information on avalanche runout distances, flow depth, and flow velocity (Fig. 2).

14

15 **3.3 GLOF process-chain modeling**

16 To estimate the future volume, we first mapped its potential maximum extent by reconstructing
17 the glacier bed using a spatially distributed glacier ice thickness product combined with a DEM
18 (see results Fig. 8a). In the absence of direct ice thickness measurements and subglacial
19 topography data, we utilized ensemble ice thickness data (Farinotti et al., 2019). Raster-based
20 calculations were performed to derive a spatially distributed glacier-bed surface. We followed
21 contour-based bathymetry generation approaches used previously in western Himalayan lake-
22 bathymetry reconstructions (Sattar et al., 2023, 2021). Lake and basin volumes were further
23 compared with volume-area scaling relationships (Cook and Quincey, 2015; Emmer and
24 Vilimek, 2014; Evans, 1986; Fujita et al., 2013; Huggel et al., 2002; Kapitsa et al., 2017;
25 Loriaux and Casassa, 2013; Muñoz et al., 2020; Wang et al., 2012).

26 To assess potential GLOF impact from Lake-B, we employed a combination of r.avaflow and
27 HEC-RAS hydrodynamic models (v5.0.7) (D. D. More et al., 2024; Mergili et al., 2017). Both
28 r.avaflow and HEC-RAS have demonstrated effectiveness in modeling outburst floods in steep
29 Himalayan terrains (Anacona et al., 2015; D. D. More et al., 2024; Klimeš et al., 2014; Sattar
30 et al., 2019; Wang et al., 2018). ALOS PALSAR DEM was also used as the terrain for the
31 GLOF simulations.



- 1
- 2 **Fig. 2.** Schematic summary of modeled scenarios for glacial lake outburst flood process chains
3 from Lake-B in the Warwan sub-basin, illustrating mass-movement triggering and propagation,
4 impact-wave formation, lake overtopping, moraine erosion, and downstream flood routing;
5 three scenarios were simulated, involving avalanche volumes of 25×10^6 , 12.5×10^6 , and 6.25
6 $\times 10^6 \text{ m}^3$.
- 7 We defined three scenarios for potential GLOF process chain modeling. Each scenario includes
8 (1) avalanche triggering and propagation, (2) avalanche impact on glacial lake and impact wave
9 generation, (3) lake overtopping, (4) moraine erosion, and (5) downstream flood propagation
10 (Fig. 2). The density of the modeled avalanche was assumed to be 2300 kg m^{-3} assuming it to
11 be potential rock-ice avalanches. The simulations for processes from 1 to 4 were performed



1 using r.avaflow, and HEC-RAS was employed to model process 5 (Fig. 2). In scenario 1 (SC-
2 1), a rock-ice avalanche of $25 \times 10^6 \text{ m}^3$ (high magnitude), similar to the Chamoli event, was
3 simulated from the headwall toward the lake (Shugar et al., 2021). Similarly, in scenarios 2 and
4 3 (SC-2 and SC-3, respectively), simulated avalanches of $12.5 \times 10^6 \text{ m}^3$ (moderate magnitude)
5 and $6.25 \times 10^6 \text{ m}^3$ (low magnitude) respectively. GLOF outflow hydrographs were extracted
6 immediately downstream of the lake (Section 1; fig. 10) for all GLOF modeled process-chain
7 scenarios. To represent a conservative approach to map downstream GLOF inundation and
8 flow hydraulics, we consider the high-magnitude (SC-1) as a worst case among all three
9 scenarios considered in the study. The GLOF-process outflow hydrograph of the high-
10 magnitude scenario (SC-1) was used as the upstream boundary condition for downstream
11 GLOF routing. We have considered only water routing downstream of section 1 because
12 modeling the deposition and erosion due to debris flow is complex and can hinder model
13 stability. The same approach was followed by Sattar et al. (2025) for reconstructing the South
14 Lhonak GLOF event in Sikkim Himalaya (Sattar et al., 2025a). A model domain extending ~ 85
15 km downstream from the lake outlet was delineated using a 1 km buffer on either side of the
16 stream. A computational mesh of 12.5 m was generated. Due to a lack of vegetation along the
17 flow channel, a Manning roughness coefficient of 0.04 was used, consistent with previous
18 Himalayan GLOF studies (Rinzin et al., 2025). Following Rinzin et al. (2025), all other
19 hydraulic and computational parameters followed default HEC-RAS settings (Rinzin et al.,
20 2025).

21 **3.4 Mapping GLOF-exposed infrastructures**

22 The hydraulic behavior of the GLOF wave in the worst-case scenario (SC-1) was analyzed at
23 different sites (section 1, section 2, and section 3) along the flow channel using modeled output
24 of flood discharge, flow depth, velocity and inundation extent. Section 2 is located 49 km
25 downstream of the lake, and section 3 is located immediately upstream of Qaderna village, ~ 65
26 km downstream of the lake. Further, the modeled GLOF outputs were overlaid onto high-
27 resolution Maxar imagery (Google Earth) to manually map exposed downstream
28 infrastructures, including bridges, buildings, road segments, and other critical assets.

29

30

31

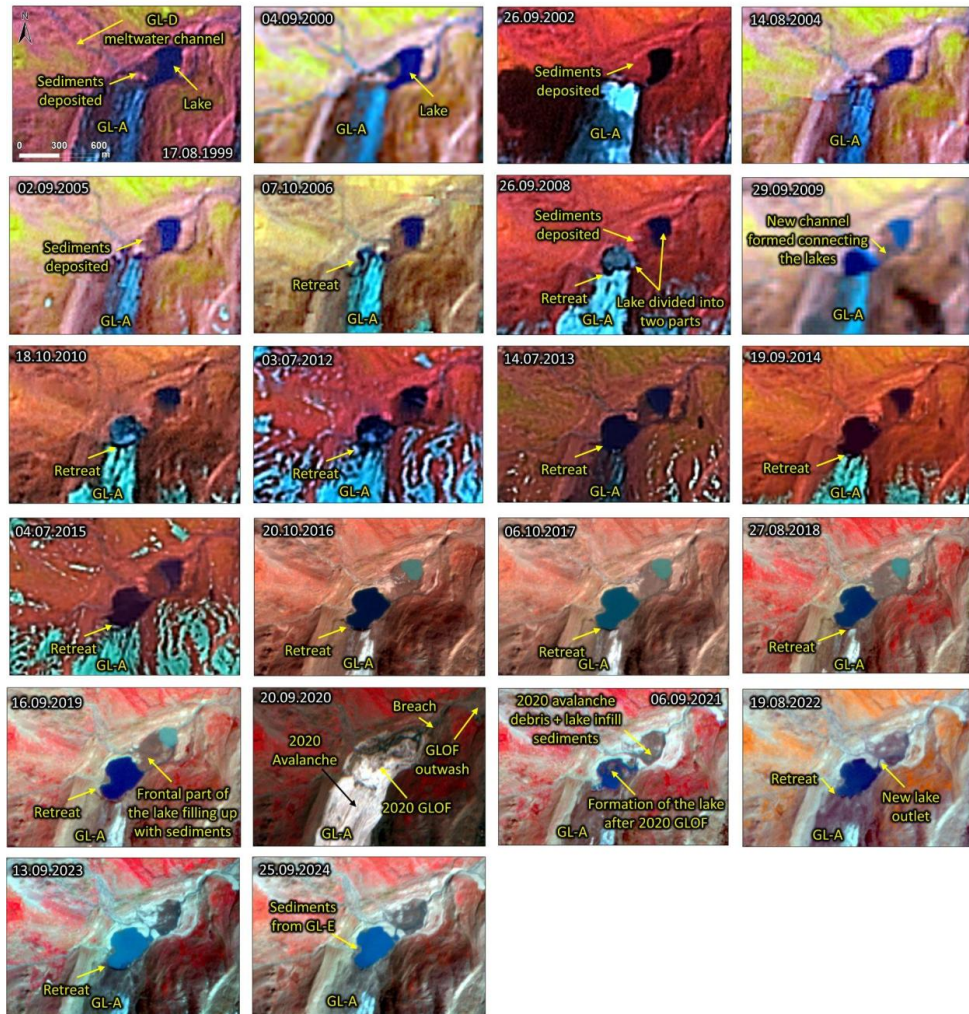


1 4 Results

2 4.1 Contrasting evolution of glacial lakes Lake-A and Lake-B

3 Analysis of multi-temporal satellite imagery indicates a clear trend of glacier retreat within the
4 glacier complex, leading to the formation and progressive expansion of glacial lakes (Fig. 3 &
5). In 1999, both glaciers, GL-A and GL-B, exhibited proglacial lakes, while meltwater from
6 GL-D and GL-E contributed to GL-A's lake system. For GL-B, differential retreat was
7 observed along its margins, with pronounced retreat along the left margin compared to the right
8 (Fig. 5a). This asymmetrical retreat appears to be driven by enhanced water-ice interactions
9 and shifts in the thermal regime, as meltwater inputs from GL-C and GL-A's lake converged
10 into GL-B's lake from the left margin (Fig. 5).

11 Over the last two decades (1999–2024), the lake associated with GL-B (Lake-B) has expanded
12 by $\sim 308\%$, from $0.075 \pm 0.057 \text{ km}^2$ in 1999 to $0.306 \pm 0.008 \text{ km}^2$ in 2024 (Fig. 5). While Lake
13 A, associated with GL-A, has expanded only by $\sim 25.61\%$ (from $0.051 \pm 0.03 \text{ km}^2$ in 1999 to
14 $0.064 \pm 0.004 \text{ km}^2$ in 2020) before the 2020 GLOF event (Fig. 3 & S1). The smaller area
15 expansion of Lake-A is also due to the partial sediment influx from glacier-fed streams entering
16 the lake on the northern bank. The sediment influx from the meltwater streams of GL-D and
17 GL-E resulted in the formation of an alluvial fan within the Lake-A basin (Figs. 3 & 4).
18 Temporal analysis of the alluvial fan area revealed a progressive and significant expansion over
19 the study period (1999–2020) (Fig. 4). In 1999, the alluvial fan covered an area of $0.0173 \pm$
20 0.008 km^2 , which increased steadily to $0.0602 \pm 0.004 \text{ km}^2$ by 2020 (expansion of $\sim 248\%$).
21 The most substantial relative expansion occurred between 1999–2004, with an increase of
22 $\sim 71\%$ (reaching $0.03 \pm 0.012 \text{ km}^2$ in 2004), likely driven by enhanced sediment supply from
23 GL-D meltwater streams and active sedimentation processes (Fig. 4). Another notable
24 expansion phase occurred between 2004–2008, indicating a $\sim 36\%$ increase ($0.04 \pm 0.013 \text{ km}^2$
25 in 2008), attributed to the continued glacier retreat and resulting sediment mobilisation.
26 Between 2008 and 2012, the alluvial fan expansion rate reduced to $\sim 10\%$ ($0.45 \pm 0.014 \text{ km}^2$ in
27 2012), indicating either decreased sediment influx or increasing stabilisation of the depositional
28 environment. Minor yet consistent expansions were observed during 2012–2016 ($\sim 17\%$) and
29 2016–2020 ($\sim 15\%$).



1

2

3 **Fig. 3.** Evolution of the proglacial lake and surrounding periglacial environment at GL-A from
4 1999 to 2024. Continuous sediment infill since 1999 led to bifurcation of the lake by 2008,
5 with a connecting channel visible in 2009; the main glacier shows consistent retreat throughout
6 the period; the 2020 imagery captures the avalanche event and the fully drained lake following
7 the GLOF. (Background images: Landsat for 1999 to 2015 and ©PlanetScope from 2016 -24)

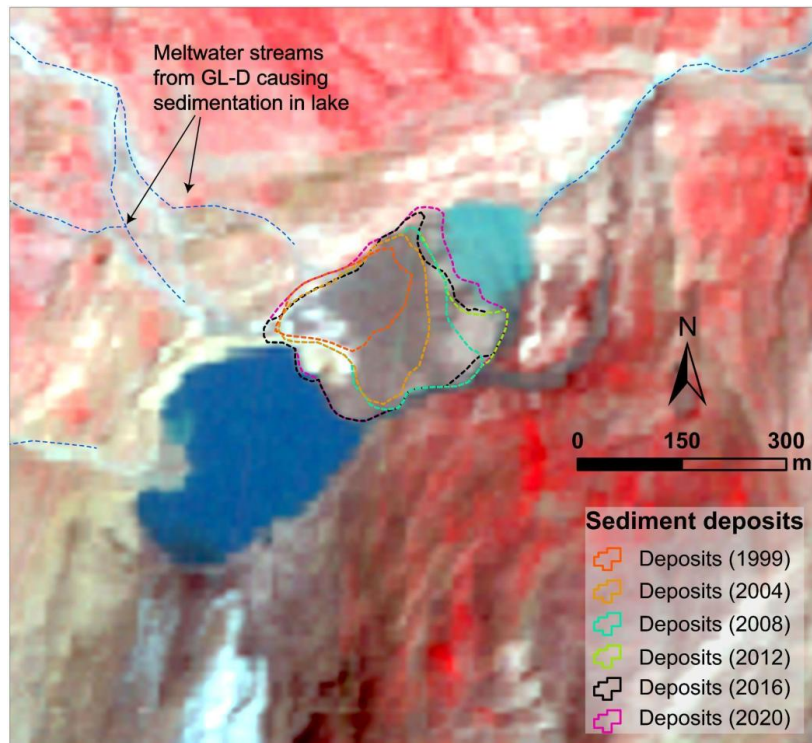
8

9 This gradually growing alluvial fan split Lake-A into two sub-basins: the fore-basin, located
10 between the moraine dam and the alluvial fan (glacier-detached since 2005), and the main
11 basin, located between alluvial fan and GL-A glacier (still proglacial in 2024). While the fore-
12 basin is visible in satellite images as early as 1999, the main basin started to evolve from small



1 supraglacial ponds in 2005-2006 (Fig. 3). The fore-basin experienced a gradual decrease in
2 area between 2013 and 2019, driven largely by sediment influx from GL-D and GL-E streams
3 draining a catchment of $\sim 8.0 \text{ km}^2$, most of which remains glacierized. After the 2020 avalanche
4 and partial breach of the dam, the fore-basin has remained water-free. In contrast, the proglacial
5 main basin experienced continued areal expansion driven by glacier retreat both before (2006-
6 2020) and after (2020-2024) the avalanche event. Notably, post-avalanche imagery reveals the
7 main basin was completely filled with ice (or floating ice) shortly after the event.

8 Assuming no sediment infill, the area of the Lake-A basin can be calculated as a sum of the
9 areas of the main basin, the fore-basin and the alluvial fan, giving a total area of $\sim 155,000 \text{ m}^2$.
10 This basin area can be converted into basin using empirical equations (Section 3.3), yielding a
11 mean basin depth of 10.7 m to 17.4 m and a total volume of $1,658,500 \text{ m}^3$ and $2,697,000 \text{ m}^3$.
12 The estimated volume of only the main basin is between 571,200 and 850,000 m^3 . These values
13 suggest that the total volume of sediment infill in Lake-A between 1999-2024 is between
14 808,500 m^3 and 2,125,800 m^3 . Considering that sediment accumulated over 25 years, the mean
15 annual sediment flux is in the order of $0.32-0.85 \times 10^5 \text{ m}^3 \text{ yr}^{-1}$ (or $0.04-0.11 \times 10^5 \text{ m}^3 \text{ yr}^{-1} \text{ km}^{-2}$).
16 If such sediment fluxes continued into the present-sized main basin, the basin may be fully
17 infilled within the next few years to decades. This highlights the short geomorphic lifespan of
18 glacier-detached high-mountain lakes in actively evolving periglacial environments (Carrivick
19 and Heckmann, 2017; Emmer, 2024).



1
2 **Fig. 4.** Sedimentation in the Lake A basin; spatial extents of sediment deposits from 1999,
3 2004, 2008, 2012, 2016, and 2020 are overlaid onto 2020 PlanetScope imagery (background
4 image: ©PlanetScope, 01.09.2020); meltwater streams from GL-D transported sediment into
5 the lake, which initially existed as a single unit until 2008 (Fig.3), later sediment deposition
6 divided the basin into the fore-basin and main-basin;
7
8

9 **4.2 Past avalanches in the region**

10 **4.2.1 Observations**

11 The September 2020 avalanche, observed in PlanetScope imagery dated 08.09.2020, triggered
12 a GLOF that led to the complete drainage of Lake-A. The rock-ice avalanche initiated from the
13 accumulation zone of GL-A at an altitude of ~4890 m asl. This ice avalanche had a total runout
14 distance of 2,355 m, with a mapped inundation area of ~0.78 km² (Figs. 3 & S1). The avalanche
15 impact completely displaced the lake water and infill sediment, generating a downstream
16 GLOF (Fig. S1). Following the event, satellite imagery revealed breaching of the Lake-A
17 moraine, extensive GLOF outwash, and subsequent deposition in the downstream channel. In
18 the months after the GLOF, melting of the ice and debris deposited within the drained basin
19



1 resulted in the reformation of a small proglacial lake in direct contact with the glacier terminus
2 of GL-A (Fig. 3 & S1).

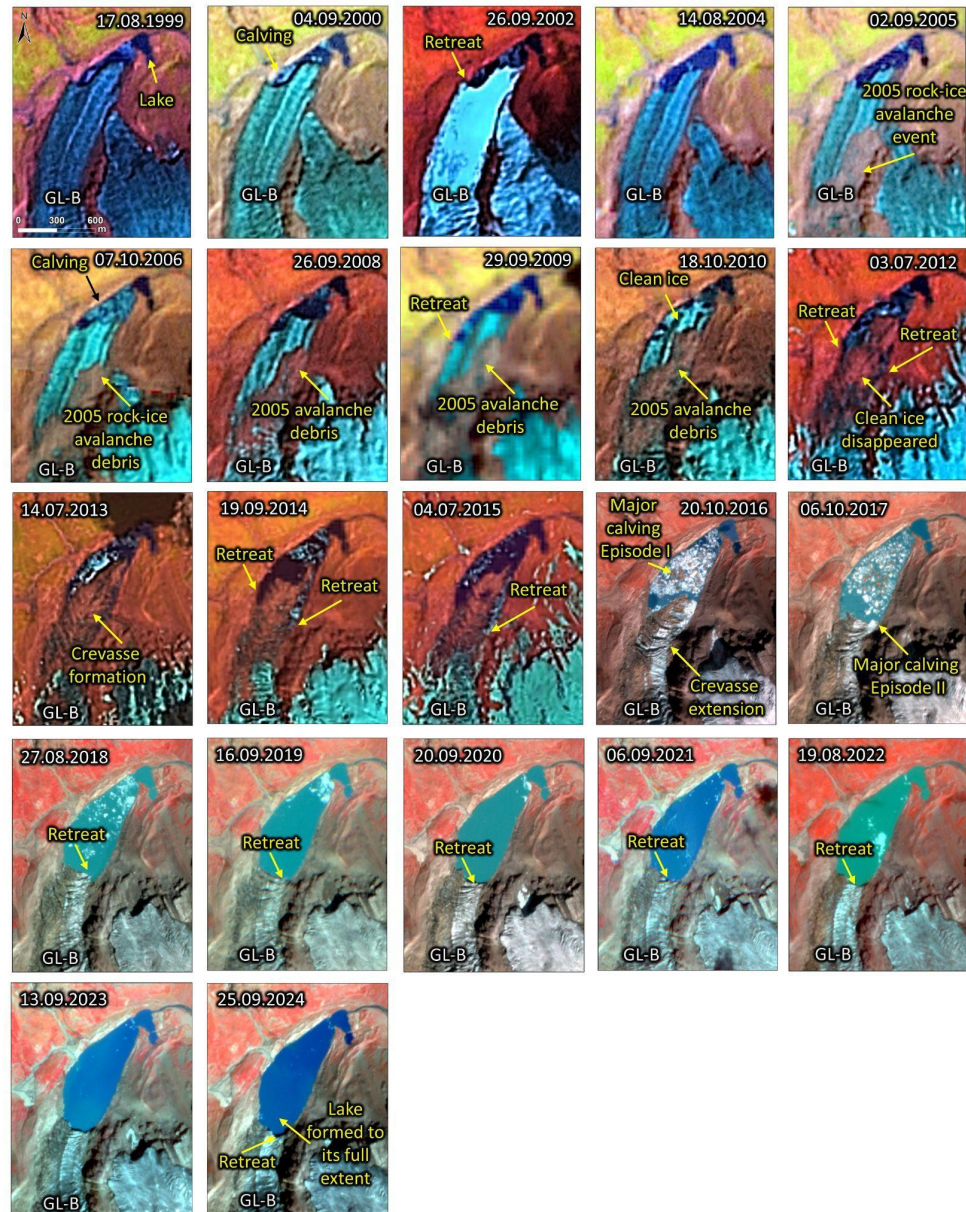
3 Again, in September 2005, satellite imagery captured an avalanche originating at an altitude of
4 ~5150 m, from the headwall of GL-B, extending ~2,620 m (inundation area of ~0.81 km²) into
5 its ablation zone (Fig. 5). However, the runout terminated before impacting the proglacial lake
6 (Fig. 5). During this period, the lake remained relatively small (~0.084 ± 0.057 km² in 2005)
7 but showed gradual lateral expansion due to frontal calving of GL-B. Concurrent with these
8 changes, one tributary of GL-B began detaching from the main trunk. Between 2013 and 2015,
9 imagery revealed water seepage emerging from the right margin of GL-B's terminus, likely
10 driven by basal melting processes (Fig. 5, in 2014-15). This seepage contributed to the
11 development of extensive crevassing across the glacier terminus, culminating in a significant
12 calving event in 2016. The following year, crevasse propagation intensified, leading to another
13 major calving episode in 2017 (Fig. 5, in 2016-17), which further contributed to lake expansion.
14 The floating ice debris observed in the lake in subsequent imagery confirms these calving
15 events. However, Lake-B has expanded ~3.6 times (from 0.09 ± 0.057 km² in 2005 to 0.306 ±
16 0.008 km² in 2024) after the September 2005 avalanche event. Owing to this, growth in lake
17 size the hazard potential of the lake needs to be assessed for its present condition (see section
18 4.3). It is also noted that another avalanche occurred in March 2020 on GL-F (see Fig. 7) which
19 experienced a rock-ice avalanche event, initiated from the headwall at ~5340 m and travelled
20 a runout distance of ~2470 m, affecting an area of ~1.24 km² along its path in the upper ablation
21 zone of the glacier. Although this avalanche did not reach a proglacial lake, its scale and
22 geomorphic impacts highlight the ongoing slope-instability processes active across the wider
23 glacier complex.

24

25

26

27



1
2 **Fig. 5** The evolution of the proglacial lake and associated processes in the periglacial
3 environment of GL-B, from 1999 to 2024; the images show the debris associated with the 2005
4 rock-ice avalanche, crevasses, glacier ice calving, and glacier retreat; ice floating on the glacial
5 lake due to calving is also visible in the imagery. (background images: Landsat for 1999-2015
6 and ©PlanetScope for 2016-24)

7

8

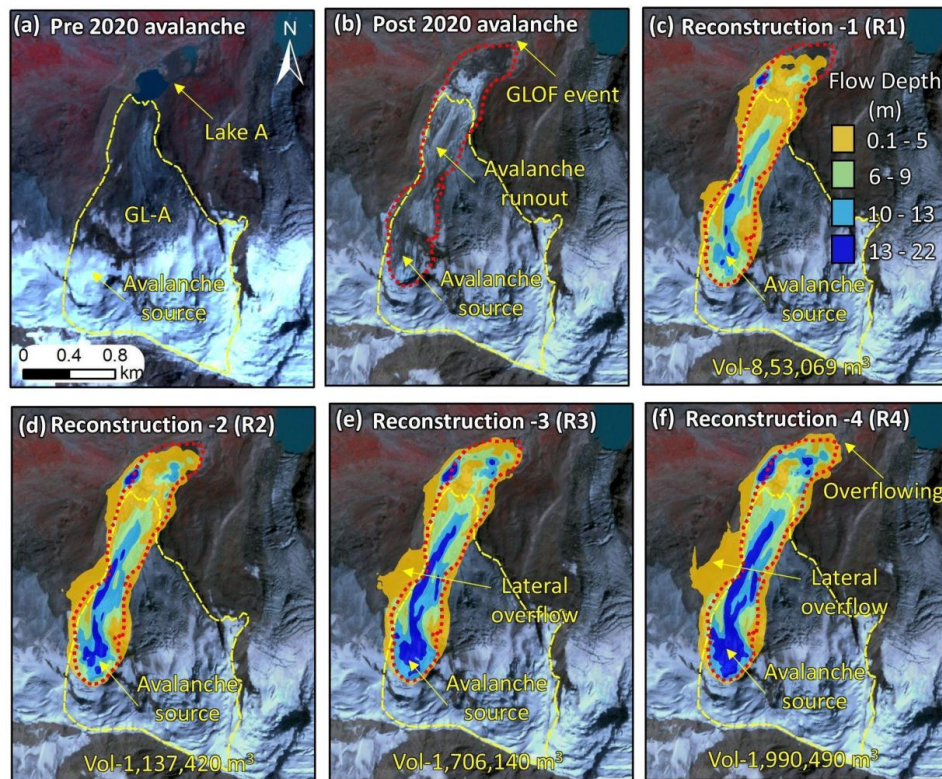


1 4.2.2 Avalanche reconstruction

- 2 The September 2020 avalanche reconstruction (that occurred on GL-A) based on various
3 release depths led to distinct variations in modeled runout behavior (Fig. 6). In scenario R1,
4 with a release volume of $8.53 \times 10^5 \text{ m}^3$, the modeled avalanche aligned well with the mapped
5 runout. Similarly, in scenario R2, using a slightly higher release volume of $1.13 \times 10^6 \text{ m}^3$, the
6 simulated runout also demonstrated a good match with the observed extent. However, as the
7 assumed release volumes were increased by ~50 % (R3) and ~75% (R4), the modeled runouts
8 exceeded the mapped deposition limits, producing unrealistic flow overshoot and indicating
9 that these larger volumes are inconsistent with actual avalanche runouts.
- 10 For the March 2020 avalanche that occurred on GL-F, reconstruction using varying release
11 depths similarly produced differing runout patterns (Fig. 7). In scenario R1, with a release
12 volume of $8.69 \times 10^5 \text{ m}^3$, the simulated runout did not adequately match the observed avalanche
13 extent. Likewise, scenario R2, with a release volume of $1.3 \times 10^6 \text{ m}^3$, also failed to reproduce
14 the mapped runout. However, when the release volumes were increased to $1.74 \times 10^6 \text{ m}^3$ (R3)
15 and $2.17 \times 10^6 \text{ m}^3$ (R4), the R4 scenario provided the best overall fit to the mapped avalanche
16 extent (Fig.7), suggesting that a larger initial failure volume is required to reproduce the
17 observed deposition pattern for this event.



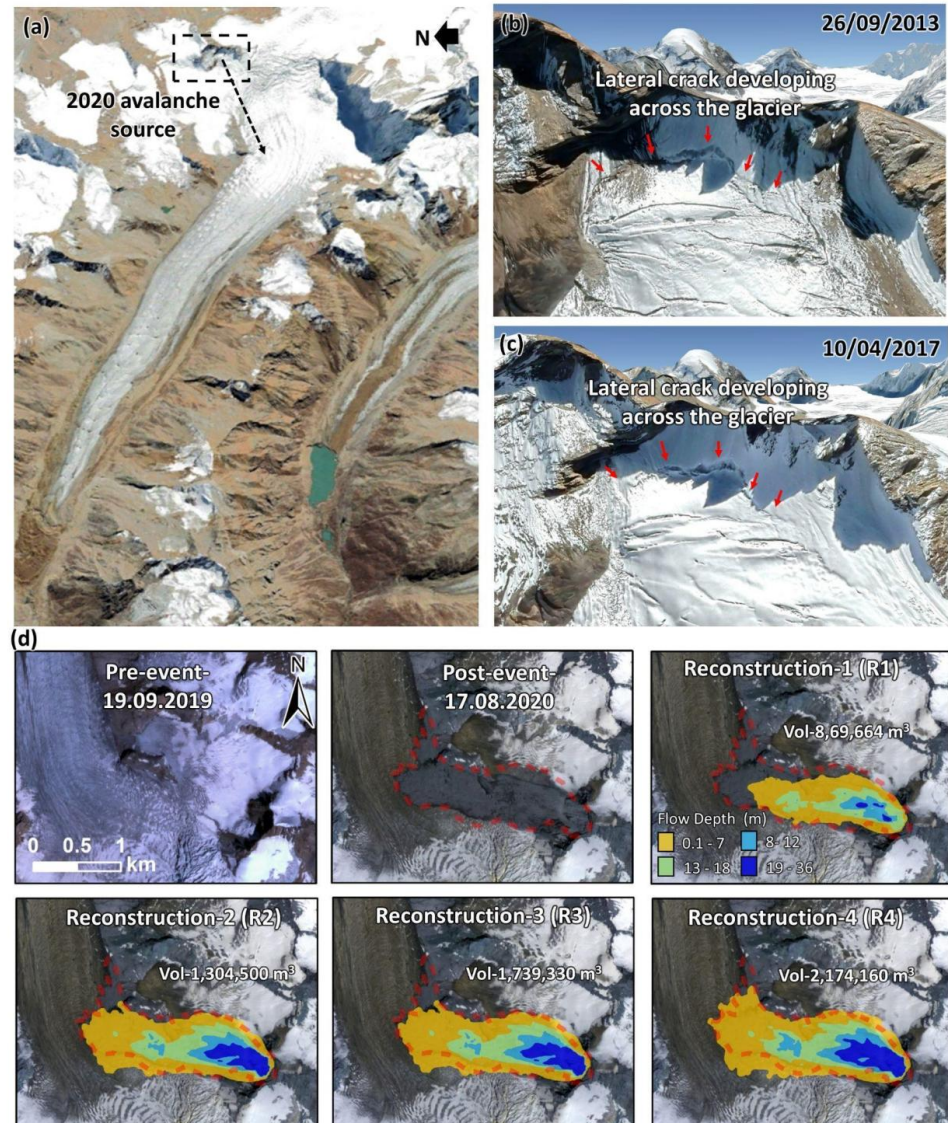
1



2

3 **Fig. 6.** Pre-GLOF PlanetScope imagery showing (a) the source zone of the 2020 avalanche
4 from GL-A that triggered the GLOF event; (b) the mapped 2020 avalanche inundation; (c-f)
5 reconstructed avalanche runouts (R1-R4) for different release volumes. Scenarios R1 and R2
6 exhibit the best fit with the actual mapped avalanche inundation; (all background image:
7 ©PlanetScope)

8



1
2 **Fig. 7.** (a-c) Pre-event Google Earth images showing the lateral crack that developed in the
3 upper reaches of GL-F, causing the 2020 avalanche. (d) Pre-event and post-event PlanetScope
4 imagery depicting the avalanche source zone, inundation area, and reconstructed runouts (R1-
5 R4). Scenario R4 showed the best fit with the actual mapped avalanche inundation.
6 (background image in a-c is © CNES/ Airbus, and d is © PlanetScope)

7

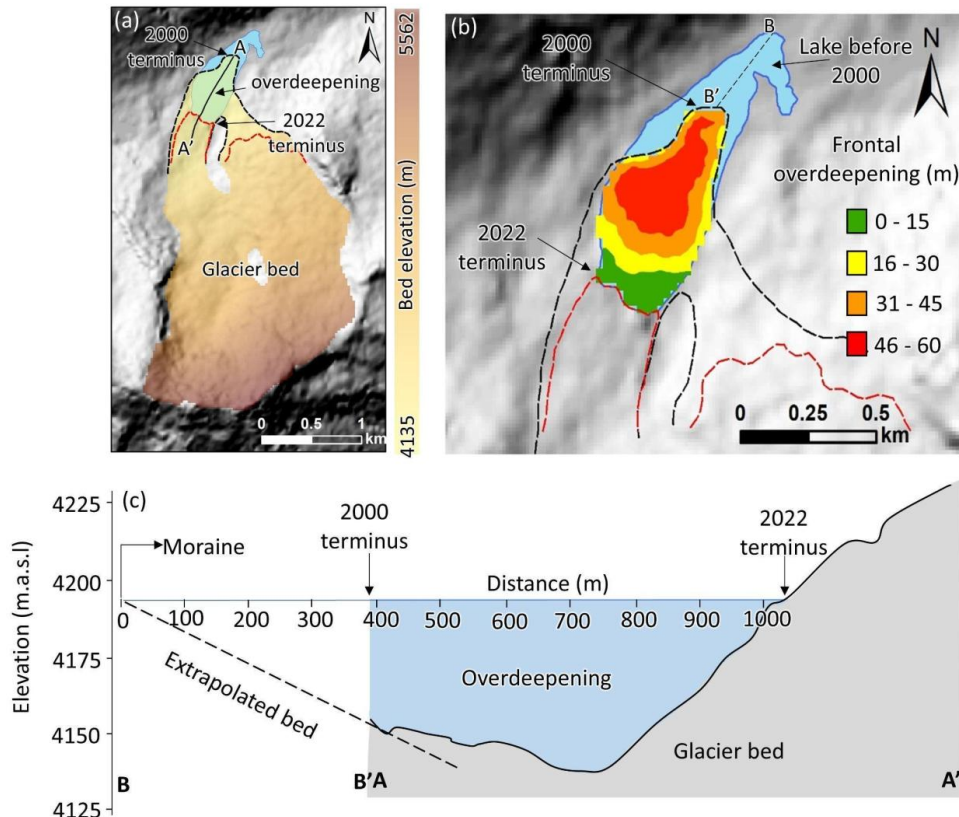
8



1 **4.3 Future avalanche-induced GLOF process chains from Lake-B and downstream**
2 **exposure**

3 Mapping of Lake-B showed exponential growth (~308%) between 1999-2024 (see section 4.1;
4 Fig. 5). Also, GL-B which is associated with this lake witnessed an avalanche in 2005 (Fig. 5).
5 To address the future GLOF hazard of the lake, the maximum possible future lake extent is
6 considered for GLOF modeling in this study. For this, the modeling of frontal overdeepening
7 of GL-B (Fig. 8a) and frontal overdeepening of Lake-B between 2000 and 2022 shows a
8 maximum depth of ~60 m, with a mean depth of 28.5 m, where a deep glacier depression is
9 observed (Fig. 8b) (section 3.3). Based on this, the maximum lake volume was calculated as
10 $7.7 \times 10^6 \text{ m}^3$. The lake volume estimated using V–A scaling approaches was $\sim 7.4 \times 10^6 \text{ m}^3$, and
11 comparison between the modeled volume and the ensemble mean of scaling results showed a
12 difference of ~4%. However, for GLOF modeling, we adopted the ice-thickness-based volume
13 estimate from Farinotti et al. (2019), as it provides robust and widely validated values and has
14 been used in recent Himalayan lake studies (e.g., (Sattar et al., 2023)). Fig. 8(c) also reveals
15 that the frontal zone of Lake-B is relatively shallow (~13 m depth), whereas the central part
16 reaches depths of ~60 m. The depth variability reflects the gently dipping lake-bed toward the
17 frontal portion. Such glacial-lake beds are typical in nature as also seen in bathymetric surveys
18 of glacial lakes in the Himalaya where the lakes are deeper near the glacier terminus and gets
19 shallower towards the front (Das and Ramsankaran, 2025; Haritashya et al., 2018; Watson et
20 al., 2020).

21



1 **Fig. 8.** (a) Spatially distributed glacier bed elevation (in m asl) of GL-B showing the lake
2 extent in 2000 (blue) and the glacier bed overdeepening extent (green); (b) Spatially distributed
3 depth of the frontal overdeepening of lake GL-B; (c) Depth profile of the overdeepening (AA')
4 along the central line of the lake GL-B and extrapolated bed profile based on the bed slope
5 extending till the frontal moraine of the lake (BB').
6

7

8 In the worst-case (large-magnitude) GLOF process chain triggered by a $25 \times 10^6 \text{ m}^3$ rock–ice
9 avalanche (SC-1) entering Lake-B, peak discharges of $2,214 \text{ m}^3 \text{s}^{-1}$ (liquid phase: lake water)
10 and $1,316 \text{ m}^3 \text{s}^{-1}$ (solid phase: avalanche debris) were generated at section-1, located
11 immediately downstream of the lake (Section 3.3; Fig. 10a). 97.5% of the water present in the
12 lake is potentially drained out of the Lake-B. In the moderate-magnitude GLOF process chain
13 (SC-2), initiated by a $12.5 \times 10^6 \text{ m}^3$ avalanche, the peak discharge at Section-1 was $1,644$
14 (water) $\text{m}^3 \text{s}^{-1}$, representing a 25% reduction and draining 91% of the lake volume. For the
15 low-magnitude scenario (SC-3), the peak discharge was $1,260 \text{ m}^3 \text{s}^{-1}$, a 43% reduction relative
16 to SC-1, draining 85.71% of the lake water. The avalanche volume deposited in the lake was 5



1 $\times 10^6 \text{ m}^3$ for SC-1, $3.1 \times 10^6 \text{ m}^3$ for SC-2, and $1.7 \times 10^6 \text{ m}^3$ for SC-3 (Table 1). For all three
2 modeled scenarios, the avalanche mass flow continued beyond the lake and was subsequently
3 deposited downstream. $18.4 \times 10^6 \text{ m}^3$ was deposited downstream of the lake in SC-1, 8.7×10^6
4 m^3 in SC-2, and $4.2 \times 10^6 \text{ m}^3$ for SC-3 (Fig. 9; Table 1).

5 GLOF routing in SC-1 showed floodwater propagating downstream and reaching Section-2
6 after ~5 hours and Section-3 after ~6 hours after the initiation of the GLOF event. The modeled
7 maximum flow depths were 2.8 m and 2 m at Section-2 and Section-3 respectively. The peak
8 discharge attenuated substantially along the flow path due to channel resistance, reducing to
9 $621 \text{ m}^3 \text{s}^{-1}$ at Section-2 and further to $535 \text{ m}^3 \text{s}^{-1}$ at Section-3 (Fig. 10b). By the time the flood
10 reaches Section-3 near the populated settlements, the peak discharge is significantly reduced
11 by 73% compared to Section-1. This emphasizes the critical role of flow attenuation over
12 distance and the influence of valley morphology, channel storage, and flow resistance along
13 the GLOF pathway.

14 The modeled worst-case GLOF scenario (SC-1) indicates that a substantial number of
15 infrastructures are at exposed, particularly those situated along the banks of the MaruSudar
16 River near Youdu and Qaderna villages. The analysis reveals that 9 bridges, 40 buildings, and
17 multiple road networks are exposed to GLOF-associated flooding (Fig. 10). GLOF flow depth
18 depths and flow velocity are reaching up to 2-4 m and $4-6 \text{ ms}^{-1}$ at places where infrastructure
19 is located.

20

21

22

23

24

25

26

27

28

29



1

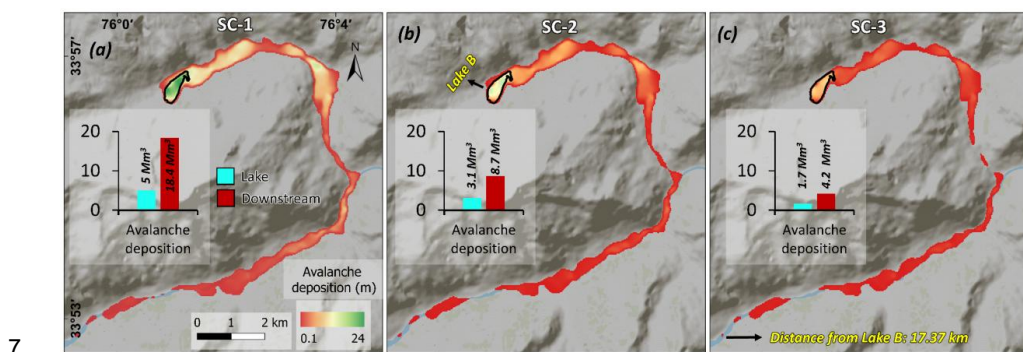
	SC-1	SC-2	SC-3
Water released from the lake (%)	~98%	~91%	~86%
Avalanche volume deposited in the lake	$5.0 \times 10^6 \text{ m}^3$	$3.1 \times 10^6 \text{ m}^3$	$1.7 \times 10^6 \text{ m}^3$
Avalanche volume overflowing lake	$20 \times 10^6 \text{ m}^3$	$9.4 \times 10^6 \text{ m}^3$	$4.5 \times 10^6 \text{ m}^3$
Magnitude	High	Moderate	Low

2 **Table 1.** Percentage of water released and the total deposition volume of avalanche in the lake
3 for scenarios SC-1, SC-2, and SC-3.

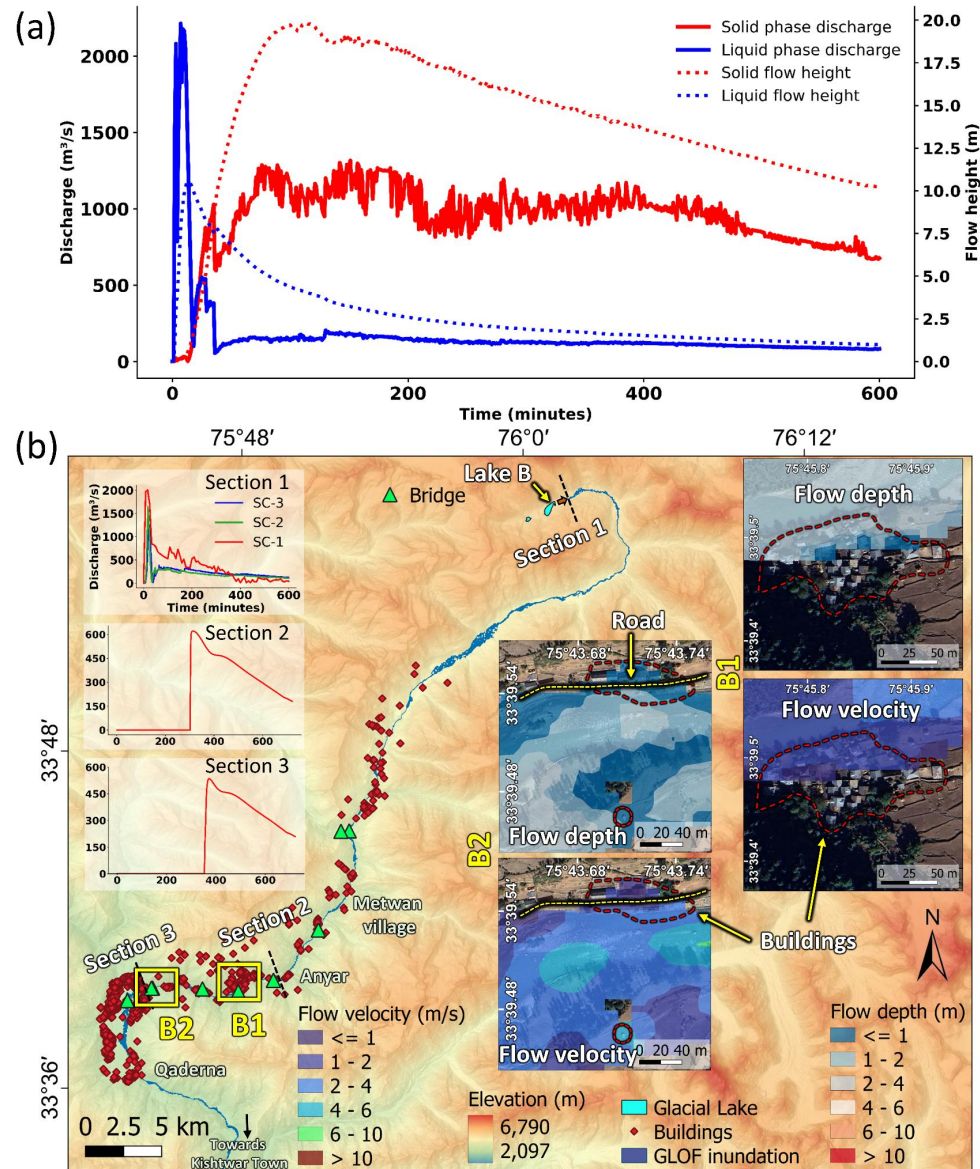
4

5

6



8 **Fig. 9.** Spatial distribution of avalanche deposition downstream of the Lake-B in scenarios (a)
9 SC-1, (b) SC-2, and (c) SC-3; avalanche deposition volumes are shown in bar charts and are
10 given in Mm^3 ($\times 10^6 \text{ m}^3$).



1 **Fig. 10.** (a) Modeled GLOF process-chain discharge and flow height versus time plot of two
2 phases: avalanche and lake water at Section 1 for SC-1; (b) modeled GLOF inundation from
3 the lake to downstream settlements at Yordu and Qaderna, in the Warwan subbasin; GLOF
4 hydrographs are extracted immediately downstream of the lake (Section 1) for all three
5 modeled process chains (SC-1, SC-2, and SC-3); routed hydrographs for the worst-case GLOF
6 (SC-1) extracted at Sections 2 and 3, at Anyar and before Qaderna; buildings and bridges are
7 overlaid on the flood inundation (SC-1) to identify the exposed infrastructure; subsets B1 and
8 B2 show flow depth and flow velocity overlaid on high-resolution imagery. (Background
9 images in the subsets are © Maxar Technologies from Google Earth)
10



1 5 Discussion

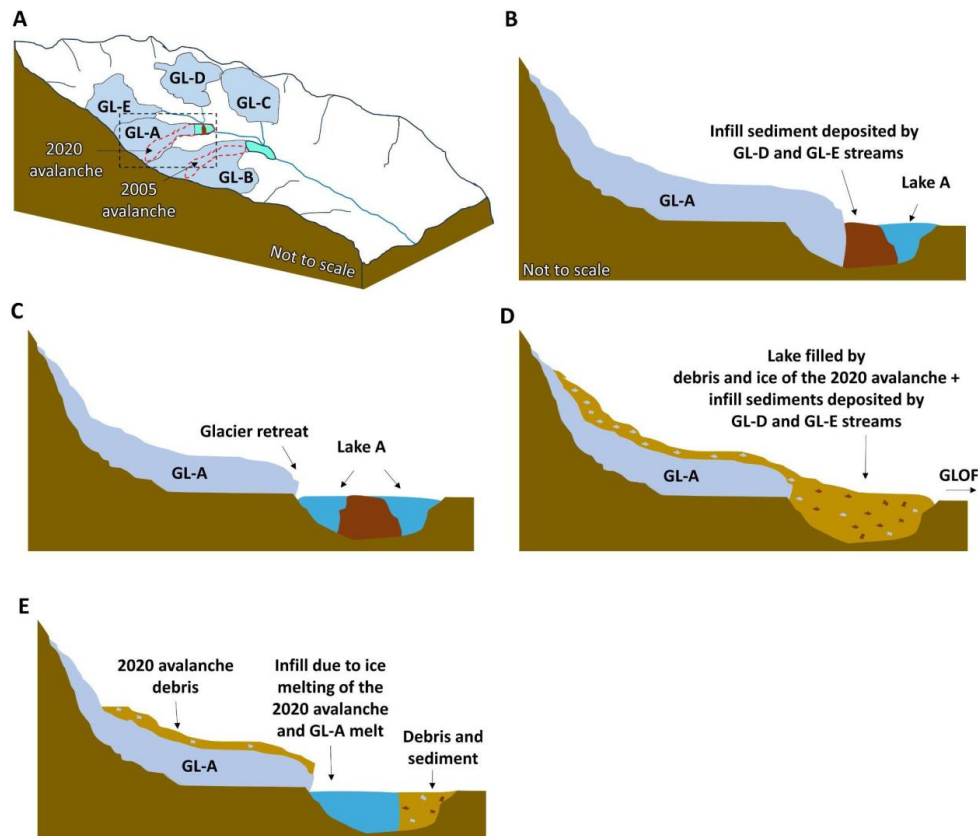
2 5.1 Unreported GLOFs in remote high mountains

3 The HKH is experiencing warming nearly twice the global average, providing favourable
4 conditions for the formation and rapid expansion of glacial lakes (Wang et al., 2015) . With
5 rising temperatures, receding glaciers, expanding glacial lakes, and degrading permafrost,
6 GLOFs have become an increasingly frequent phenomenon across the HKH. The frequency of
7 GLOFs is expected to rise further as a lagged response to the rapid expansion of glacial lakes,
8 drawing parallels to the lagged response to post-Little Ice Age warming during the 1930s
9 (Harrison et al., 2018). Zheng et al. (2021) reported that at least 21 GLOF events occurred per
10 year in the region from 1900 to 2016, with the majority being unreported (Zheng et al., 2021a).
11 A regional inventory of unreported GLOF revealed that 57% (101 events) occurred in the
12 Himalaya, highlighting the region as a global hotspot for unreported GLOFs (Zheng et al.,
13 2021a).

14 In the remote Himalayan region, GLOFs and mass movement events often remain unreported
15 (Veh et al., 2022, 2019), due to their limited downstream impact and subtle geomorphic
16 signatures. In the case of Lake-A, the unreported 2020 outburst can be attributed to multiple
17 interlinked factors. First, the outburst released a low water volume, as sediment infilling and
18 reduced meltwater inputs had substantially decreased the lake's storage capacity prior to failure
19 (Emmer, 2024). Consequently, the resulting flood lacked the hydraulic force necessary to
20 induce significant geomorphic disturbances such as extensive channel erosion, debris fans, or
21 bank destabilization that typically serve as visible evidence of past GLOFs (Lützow et al.,
22 2023). Second, the absence of any notable damage to downstream infrastructure or settlements
23 contributed to its invisibility in hazard records and local knowledge systems (Emmer et al.,
24 2020; Emmer and Cochachin, 2013; Zheng et al., 2021a). Emmer and Vilímek (2014) also
25 highlighted that small-volume outburst floods are often unreported, especially in sparsely
26 populated regions with minimal monitoring networks (Emmer and Vilímek, 2014).
27 Additionally, if the outburst flow is rapidly attenuated within short downstream distances due
28 to channel storage, infiltration, or debris-dominated flow regimes, its cascading impacts may
29 be negligible and undetectable through satellite-based geomorphic change analysis (Allen et
30 al., 2022; Dubey et al., 2024).



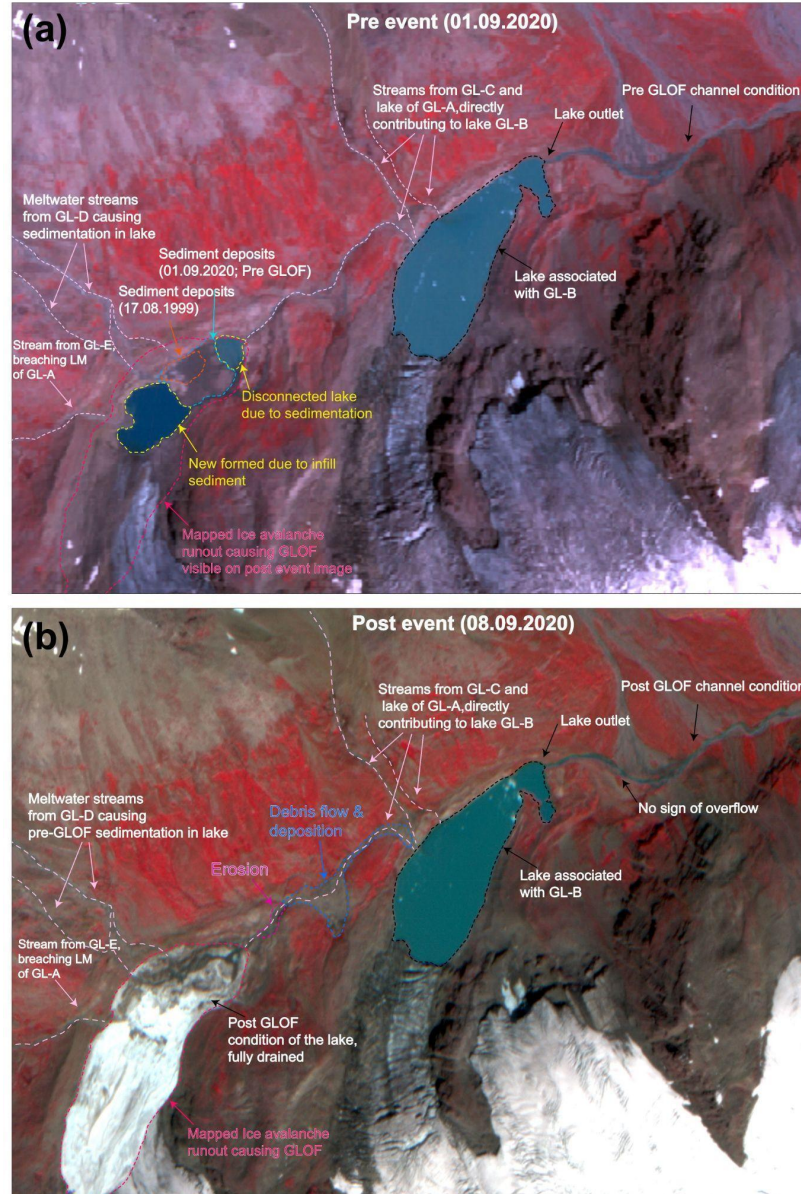
1 The September 2020 GLOF from GL-A, initiated by an ice avalanche originating from its
2 headwall, exemplifies the complex interplay between cryospheric processes and cascading
3 hazards in high mountain regions (Sattar et al., 2022). Although this event breached a small
4 proglacial lake (Lake-A) (Fig. 11), its downstream impact remained negligible. This reduced
5 storage capacity resulted from significant sediment infilling and meltwater contributions from
6 surrounding glaciers, which progressively lowered the effective reservoir volume prior to the
7 outburst. Similar sediment infilling dynamics have been reported by Emmer (2024), who
8 suggested that such processes can rapidly diminish lake storage capacity and, in some cases,
9 lead to the disappearance of glacial lakes, thereby reducing their hazard potential (Emmer,
10 2024).



11
12 **Fig. 11.** Schematic showing (A) the glacier valley and the glacier complex (GL-A, GL-B, GL-
13 C, GL-D, and GL-E) and the glacier where the 2005 and 2020 avalanche-triggered GLOF
14 occurred; (B-C) process showing the evolution of GL-A glacial lake before the 2020 avalanche
15 impact; (D) the 2020 avalanche filling up the lake basin completely, draining the lake, and
16 causing a GLOF event.



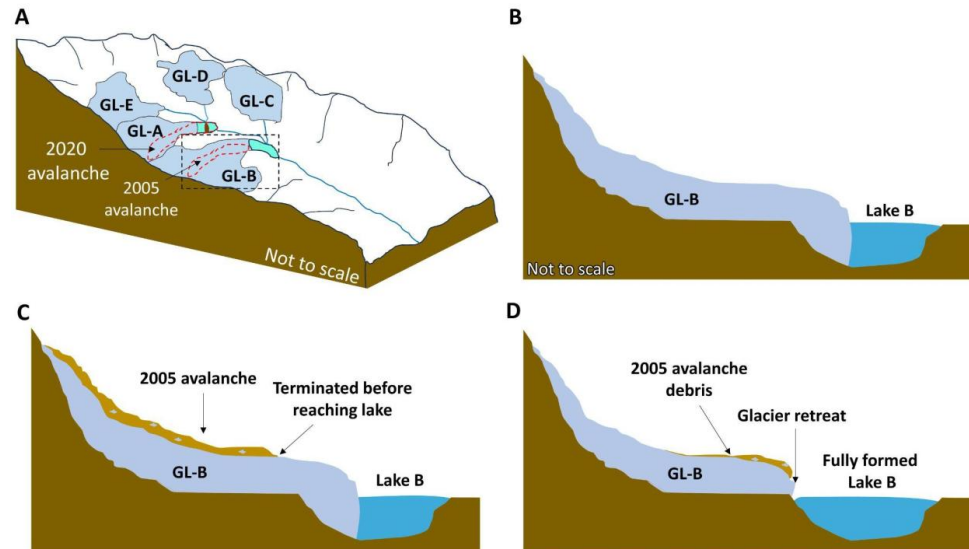
1 However, the reformation of the lake in the same basin post-2020 (Fig. 3 & S1), coupled with
2 ongoing sediment influx from adjacent glacier meltwater streams such as GL-E (Fig. 12),
3 presents a renewed risk for future outbursts (Sattar et al., 2025a). While sedimentation may
4 temporarily reduce hazard potential by lowering lake volume (Emmer and Cochachin, 2013;
5 Worni et al., 2013), it can also create a false sense of stability if dynamic geomorphic and
6 cryospheric processes are not regularly monitored (Emmer et al., 2025; Sattar et al., 2025a). Of
7 particular concern is permafrost degradation, known to destabilize headwalls and slopes,
8 facilitating rock and ice avalanches that can trigger lake breaches (Gruber, 2012; Haeberli et
9 al., 2007; Hjort et al., 2022; Huggel et al., 2008).



1
2 **Fig. 12** Geomorphic process in the periglacial environment of Lake-A and Lake-B. (a) pre-
3 GLOF scenario where the lake is visible with sediment deposits dividing it into two, and (b)
4 post-GLOF scenario where avalanche deposits are visible and the lake is completely drained
5 with no water present. Erosion immediately downstream of the lake and deposition of debris
6 is also visible (Background images are © PlanetScope)



- 1 The proximity of Lake-A to Lake-B, only a few hundred meters downstream (Fig. 11-13),
2 further elevates the potential of cascading hazard. Unlike Lake-A, Lake-B shows no visible
3 sediment infill (Fig. 12) and has expanded significantly (~ 308 %) over 25 years, retaining a
4 substantial water volume. This adjacency raises concern for cascading hazards: a slope failure
5 or avalanche into Lake-A could produce sufficient flood momentum to impact Lake-B,
6 potentially triggering sequential outburst. Westoby et al. (2014) highlighted that ice-calving
7 and avalanche-induced displacement waves are known triggers of outburst floods (Westoby et
8 al., 2014). Worni et al. (2013) similarly emphasized that lakes with minimal sediment infill
9 remain at higher hazard potential due to larger water storage (Worni et al., 2013).
- 10 Observations confirm that the GLOF and debris flow from Lake-A in 2020 did not affect Lake-
11 B's geomorphology, as no evidence of flooding or erosion were detected downstream of Lake-
12 B (Figs. 12 and 13). Nevertheless, the compounded-risk scenario remains significant where a
13 single mass movement could (i) trigger a GLOF from Lake-A, (ii) transport substantial debris
14 loads that enhance downstream flood intensity, and (iii) destabilize the moraine dam of Lake-
15 B through either hydraulic or mechanical erosion. Such multi-lake cascading hazards can
16 produce impacts far beyond those of single-lake outbursts (Harrison et al., 2018). Lake-B did
17 experience a rock/ice avalanche in 2005; however, the lake was smaller at that time, and the
18 avalanche stopped in the ablation zone before reaching the lake (Fig. 5). In contrast, by 2024,
19 Lake-B has attained its full extent, and if an avalanche of similar magnitude to that of 2005
20 were to occur under current conditions, it would directly impact the lake, potentially triggering
21 a hazard cascade downstream (Fig. 13).
- 22 Time series analyses show that Lake-B receives significant meltwater from GL-C and GL-A
23 (Fig. 12), and PlanetScope imagery indicates large transverse crevasses and floating ice chunks
24 within the lake, signifying active calving (Fig. 5). A large calving event with higher magnitude
25 to those in 2016 and 2017 (Fig. 5) could rapidly displace water, generating displacement waves
26 capable of overtopping the moraine dam and triggering an outburst (Westoby et al., 2014).
- 27
- 28
- 29



1 **Fig. 13.** Schematic showing (A) the glacier valley and the glacier complex (GL-A, GL-B, GL-
2 C, GL-D, and GL-E) and the glacier where the 2005 and 2020 avalanche-triggered GLOF
3 occurred; (B) process showing the evolution of GL-B glacial lake before the 2005 avalanche;
4 (C) the 2005 avalanche terminated before lake impact on GL-B; (D) the GL-B lake grew to its
5 full extent.

6
7
8
9 The Lake-B present a potential GLOF risk to downstream villages such as Metwan, Quadarna,
10 Anyar, and Yordu, located approximately 50–55 km downstream of the lake. Two major
11 hydropower project sites (Bursar; 800 MW and Pakal Dul; 1000 MW) are around 90 km away
12 from the lake. Though potential GLOF flow would reach a steady flow at these locations,
13 transported debris and water volume can adversely impact these sites. High-resolution imagery
14 shows that several settlements have emerged near the river in the past two decades (Fig. 10).
15 Additionally, new hydropower projects can lead to further population growth in this valley to
16 meet the region's energy demand, potentially exposing them to considerable GLOF risks in the
17 future. This spatial pattern of exposure underscores the urgent need for community-level early
18 warning systems, strategic GLOF mitigation for highly exposed settlements, and resilient
19 infrastructure design to mitigate the potentially devastating impacts of future GLOF events in
20 the region.

21

22

23

24



1 **5.2 Permafrost degradation and avalanche formation in the Warwan sub-basin**

2

3 The progressive increase in regional temperature directly influences permafrost stability in
4 high-altitude glacierized catchments (Gruber et al., 2017), including the glacier complex
5 studied here. This warming leads to the progressive degradation and thawing of ice-rich
6 permafrost interface along steep headwalls and valley flanks (Gruber and Haeberli, 2007;
7 Nicolsky and Romanovsky, 2018). Gruber and Haeberli (2007) emphasized that thawing
8 permafrost results in a loss of cohesive strength within rock-ice mixtures, enhancing slope
9 instability, exacerbating surface deformation, and promoting rockfall and rock-ice avalanches
10 (Gruber and Haeberli, 2007). The avalanche events reported in this study might also be linked
11 to the ongoing permafrost degradation. Fig. S2 shows permafrost probability and active layer
12 temperatures (Ran et al., 2022) in the catchment, both of which indicate increasingly unstable
13 ground conditions. This information is particularly relevant for the September 2005 and
14 September 2020 events, which occurred on GL-B and GL-A, respectively. Both glaciers are
15 fed by the steep headwalls underlain by permafrost, where warming-induced reduction in
16 intergranular ice cohesion could have triggered detachment of ice masses and rock blocks
17 (Fischer et al., 2012; Haeberli et al., 2010).

18

19 Recent observations show avalanches originating from the headwall region of both GL-A and
20 GL-B. These events strongly suggest that permafrost degradation might have played a critical
21 role in destabilising frozen rock masses, ultimately leading to failure initiation (Fig. S2) (Stoffel
22 et al., 2024). Such permafrost-related slope failures can further modify glacier dynamics by
23 depositing debris onto glacier surfaces, increasing surface loading, and modifying ice flow
24 patterns, as observed during the Blatten rock-ice avalanche in the Swiss Alps in 2025 (Islam et
25 al., 2025; D. Yang et al., 2025).

26

27 We reconstructed two recent avalanche events in the Warwan sub-basin, estimating release
28 volumes of $1.13 \times 10^6 \text{ m}^3$ (September 2020) and $2.17 \times 10^6 \text{ m}^3$ (March 2020). These magnitudes
29 are comparable to GLOF-triggering avalanches in other mountain ranges such as Cordillera
30 Blanca ($0.2\text{--}0.4 \times 10^6 \text{ m}^3$) (Worni et al., 2014) and the Tibetan plateau ($3.8 \times 10^6 \text{ m}^3$) (L. Yang
31 et al., 2025). In IHR, studies indicate that avalanches with release volumes exceeding 0.5×10^6
32 m^3 are typically required to trigger a GLOF (Abhinav and Sattar, 2025; Rounce et al., 2017).
33 In this study, avalanche reconstruction relied primarily on mapped spatial extents, due to the
34 absence of field-measured snow/ice thickness, deposit depth, or density data. As a result, the



1 reconstructed release depths and velocities carry uncertainty, and matching modeled versus
2 observed deposit characteristics remains a challenge. Future studies integrating drone surveys,
3 LiDAR, or field-based measurements of avalanche debris depth and flow indicators would
4 greatly improve parameter estimation (Abhinav and Sattar, 2025).

5
6 Permafrost degradation is expected to continue under current warming trends, further
7 weakening slope stability and increasing the likelihood of repeated avalanche activity in the
8 catchment. The combination of repeated ice avalanches (volumes $> 0.5 \times 10^6 \text{ m}^3$), steep
9 permafrost-degrading headwalls, and expanding glacial lakes in the sub-basin pose a serious
10 and evolving GLOF hazard. As Lake-A has re-formed following the 2020 event, the renewed
11 presence of a lake increases the likelihood of future avalanche-triggered GLOFs, raising
12 concern over potential cascading hazards in the region.

13
14 **5.3. Potential for future debris flow in the valley**
15

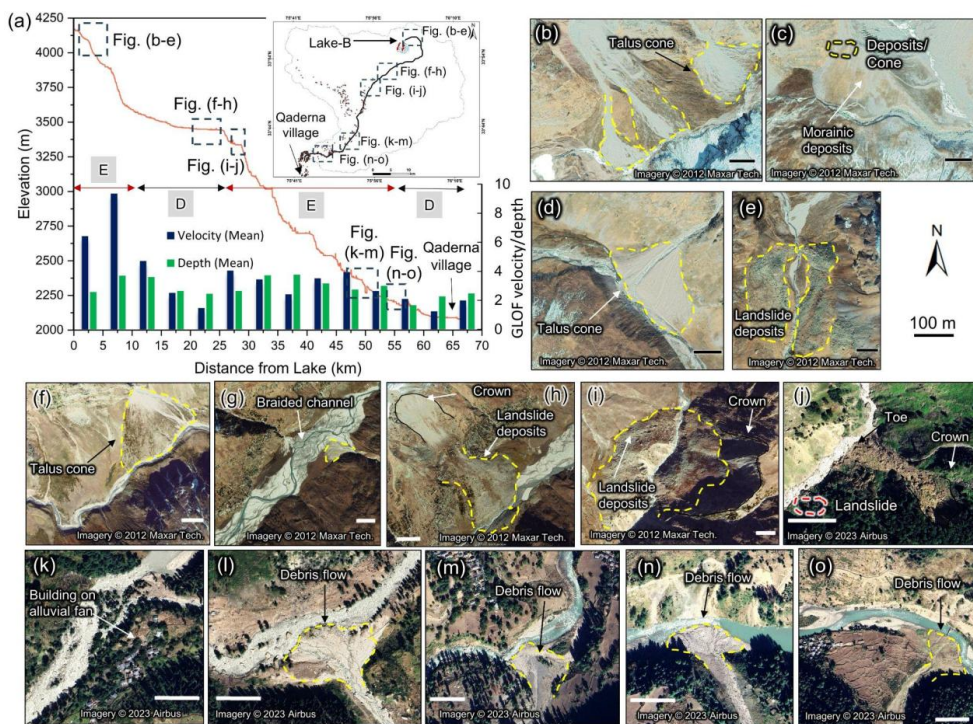
16 The catchment shows clear geomorphic evidence of past mass-wasting processes, including
17 debris flows and rock slides, particularly along the river course, which originates from the
18 proglacial lake (Fig. 14) (Rai et al., 2025). Historical slope failures, including large rock slides
19 (Fig. 14 d, g, h), appear to have disrupted river flow periodically, suggesting a long history of
20 landscape instability. More recent debris flows, likely triggered by intense monsoonal
21 precipitation (Fig. 14 j–n), further demonstrate the catchment's sensitivity to
22 hydrometeorological forcing. These processes have contributed to a significant accumulation
23 of unconsolidated sediments along the valley, increasing the potential for future sediment
24 remobilization. In this context, a future GLOF could act as a high-magnitude trigger (multi-
25 fold hazard cascade), mobilizing existing debris and initiating extensive downstream debris
26 flows (Emmer et al., 2025; Sattar et al., 2023; Yanites et al., 2025). The combination of steep
27 topography, readily available loose material, and hydrological triggers indicates that the
28 catchment is already predisposed to cascading hazards. Modeled GLOF from Lake-B shows
29 that flow would encounter alternate steep and gentle slopes (Fig. 14a). The major portion of
30 the valley along the GLOF flow path is steep which will allow high energy flows and thus more
31 erosion. Thus, any future GLOF event in the valley is unlikely to occur in isolation; instead, it
32 may initiate a sequence of hazards, including debris flows, temporary channel blockages, and
33 subsequent downstream flooding. However, in the current study, we have modeled only the
34 downstream water routing, as modeling the complex interplay between sediment erosion and



1 deposition in the case of a debris flow from the lake is challenging and requires further
2 investigations. This underscores the importance of assessing compound and cascading hazard
3 interactions rather than focusing solely on isolated processes when evaluating risk in
4 glacierized catchments.

5

6



7
8 **Fig 14.** The elevation profile of the GLOF flow channel and the modeled average GLOF
9 velocities and depth at 5 km intervals; potential zones of erosion (E) and deposition (D) are
10 marked based on GLOF hydraulics and the slope of the valley; (b-o) high-resolution imageries
11 showing previous mass movement events and their deposits at various locations along the
12 potential GLOF path from Lake-B. (Background images in b-o are © Maxar
13 Technologies/CNES/Airbus)



5.4 Socio-Economic factors of GLOF exposure and vulnerability:

The GLOF inundation map (Fig. 10), prepared based on a potential worst-case GLOF scenario, demonstrates that most infrastructures located along the flow channels of the Fariabad Nallah and MaruSudar River fall within the GLOF inundation zone. Notably, road networks and residential buildings near the riverbanks of Fariabad Nallah, at Anyar and Rinaie villages, fall within these GLOF zones due to their immediate proximity to the river course.

The exposure and vulnerability of communities to GLOFs are deeply rooted in the socio-economic characteristics of affected regions. Numerous studies (Carrivick and Tweed, 2016; Khanal et al., 2015) highlight that settlements in high mountain environments are inherently exposed due to their proximity to glacial lakes and dependence on valley-bottom resources. The concentration of infrastructure, such as hydropower facilities, bridges, and road networks, along river corridors significantly amplifies economic exposure, as seen in previous GLOF disasters in Bhutan (Komori et al., 2012), Nepal (Cook et al., 2018; Sattar et al., 2025b), and more recently in Uttarakhand (Shugar et al., 2021) and Sikkim (Sattar et al., 2025a).

Vulnerability, however, is shaped not only by physical exposure but also by socio-economic capacities such as income level, education, access to resources, social networks, and institutional preparedness (Huggel et al., 2015). Marginalised and economically weaker communities are disproportionately vulnerable, as their limited adaptive capacity restricts proactive risk reduction measures (Carey et al., 2012). For example, dependence of the local economy on agriculture along floodplains and limited access to early warning systems increase both direct and indirect risks (Shrestha et al., 2010). In this region, increasing agricultural expansion and newly built infrastructure along the floodplain exacerbate exposure, placing more households and assets directly in harm's way.

For hazard mapping at villages such as Qaderna, Yurod, Anyar, and Rinaie, which are located along the shoreline of the flow channel, the baseflow contribution was assumed negligible relative to the hydraulic force generated by the outburst flood. However, it is important to acknowledge that in a high-magnitude scenario, the addition of baseflow to the GLOF peak discharge would cumulatively increase the total flow volume, potentially resulting in elevated water levels and enhanced flood stage (Carrivick and Tweed, 2016; Veh et al., 2020). This could marginally expand the inundation extent, particularly in confined channel reaches or low-lying areas adjacent to the river, thereby intensifying the hazard levels faced by these settlements and increasing the vulnerability of infrastructure situated close to the riverbanks.



GLOF modeling of Lake-B shows the arrival time at Anyar and Qaderna is 5 hours and 6 hours respectively in SC-1. We understand that the GLOF hydraulics and arrival times are sensitive to the process chains and the modeling approaches. Thus, leaving the possibility of lower warning times in case of different GLOF processes of Lake-B. However, an early warning system closer to the source (Lake-B) will be able to provide a good lead time in case of potential GLOF warnings. Also, for a conservative approach effective adaptation requires integrated approaches that combine glacial lake hazard assessments with community-based vulnerability evaluations and social protection policies. Such approaches can reduce exposure while enhancing resilience in vulnerable high-mountain communities. All of the downstream infrastructure, including settlements, roads, bridges, and hydropower projects, is located along the potential GLOF path from Lake-B. Therefore, actively monitoring the evolution of this glacier-lake complex and conducting GLOF hazard assessment is crucial, given the number of downstream settlements and potential exposure of critical infrastructure.

6. Conclusion

This study provides a comprehensive understanding of the evolving cryospheric and geomorphic processes in the Warwan sub-basin over the past two and a half decades. Multi-temporal satellite analyses revealed significant glacier retreat, particularly for GL-A and GL-B, contributing to the expansion of associated proglacial lakes. Lake-B exhibited a remarkable growth of ~308% between 1999 and 2024, primarily due to glacier retreat, meltwater inflow, and successive calving events. In contrast, Lake-A showed a modest expansion (~26%) until it was completely drained in the 2020 GLOF event, triggered by an ice avalanche entering the lake. Permafrost distribution in the region suggests that permafrost warming can play a significant role in triggering mass-wasting processes and promoting the destabilization and degradation of steep slopes. Future GLOF modeling suggests Lake-B poses a substantial downstream GLOF risk in the valley. Despite attenuation along the flow path, vulnerable downstream settlements, including Youdu and Qaderna, face significant flood exposure. GLOF exposure assessment reveals that numerous bridges, residential structures, and road segments lie within modeled inundation zones. The possibility of GLOF to debris flow cascades is very high in the valley owing to the available sediment for remobilization, which in turn can pose higher risk to downstream infrastructure and hydropower.

The findings emphasize the dynamic interplay between glacier retreat, sedimentation, lake expansion, and avalanche activity in shaping GLOF hazards in the Warwan sub-basin. The



results underscore the critical need for integrated monitoring of cryospheric processes, improved early warning systems, community-based preparedness, and robust mitigation strategies to safeguard life, livelihoods, and infrastructure in the region.

Acknowledgement

The authors are grateful to IIT Bhubaneswar for providing infrastructure to carry out this research. AE acknowledges the support from the HINTERLANDS project (High mountains in the Anthropocene: from landscape dynamics to hazards and risks; PRIMUS/25/SCI/005), realized at the Charles University, Faculty of Science; and Johannes Amos Comenius Programme (P JAC), project No. CZ.02.01.01/00/22_008/0004605, Natural and anthropogenic georisks. UKH was supported by the NASA High Mountain Asia grant 80NSSC24K1554. SD was supported by the Department of Science and Technology (DST), GOI with sanction no. DST/CCP/HICAB/SN- J&K/173/2018(G). AS is supported by the DST Inspire Faculty Fellowship.

Code and data availability

All the data used in this research is available online. The shell scripts used for GLOF modeling can be obtained from the first author based on request.

Author contributions

AS and SSR conceptualized this study. AS, SSR, and AA wrote the original draft of the manuscript. AS, SSR, AA, SD, and AE undertook visualization and data analysis. AS and AA performed GLOF simulations. SSR, SD, AE, UKH, and MFA carried out morphological mapping, provided insights and reviewed the manuscript.

Competing interests

The contact author has declared that none of the authors has any competing interests.

Financial support

AE was financially supported by the Johannes Amos Comenius Programme (P JAC), project No. CZ.02.01.01/00/22_008/0004605, Natural and anthropogenic georisks.



References

- Abhinav, A., Sattar, A., 2025. Snow avalanche susceptibility, hazard, and exposure assessment in the Western Himalaya using machine learning and numerical modelling. *Sci. Rep.* 15, 38093. <https://doi.org/10.1038/s41598-025-22051-w>
- Ahmed, R., Ahmad, S.T., Wani, G.F., Mir, R.A., Ahmed, P., Jain, S.K., 2022. High resolution inventory and hazard assessment of potentially dangerous glacial lakes in upper Jhelum basin, Kashmir Himalaya, India. *Geocarto Int.* 37, 10681–10712. <https://doi.org/10.1080/10106049.2022.2038693>
- Allen, S.K., Rastner, P., Arora, M., Huggel, C., Stoffel, M., 2016. Lake outburst and debris flow disaster at Kedarnath, June 2013: hydrometeorological triggering and topographic predisposition. *Landslides* 13, 1479–1491. <https://doi.org/10.1007/s10346-015-0584-3>
- Allen, S.K., Sattar, A., King, O., Zhang, G., Bhattacharya, A., Yao, T., Bolch, T., 2022. Glacial lake outburst flood hazard under current and future conditions: worst-case scenarios in a transboundary Himalayan basin. *Nat. Hazards Earth Syst. Sci.* 22, 3765–3785. <https://doi.org/10.5194/nhess-22-3765-2022>
- Anacona, P.I., Mackintosh, A., Norton, K., 2015. Reconstruction of a glacial lake outburst flood (GLOF) in the Engaño Valley, Chilean Patagonia: Lessons for GLOF risk management. *Sci. Total Environ.* 527–528, 1–11. <https://doi.org/10.1016/j.scitotenv.2015.04.096>
- Ashraf, A., Naz, R., Iqbal, M.B., 2017. Altitudinal dynamics of glacial lakes under changing climate in the Hindu Kush, Karakoram, and Himalaya ranges. *Geomorphology* 283, 72–79. <https://doi.org/10.1016/j.geomorph.2017.01.033>
- Azam, M.F., Wagnon, P., Berthier, E., Vincent, C., Fujita, K., Kargel, J.S., 2018. Review of the status and mass changes of Himalayan-Karakoram glaciers. *J. Glaciol.* 64, 61–74. <https://doi.org/10.1017/jog.2017.86>
- Bhattacharya, A., Bolch, T., Mukherjee, K., King, O., Menounos, B., Kapitsa, V., Neckel, N., Yang, W., Yao, T., 2021. High Mountain Asian glacier response to climate revealed by multi-temporal satellite observations since the 1960s. *Nat. Commun.* 12, 4133. <https://doi.org/10.1038/s41467-021-24180-y>
- Bolch, T., Kulkarni, A., Kääb, A., Huggel, C., Paul, F., Cogley, J.G., Frey, H., Kargel, J.S., Fujita, K., Scheel, M., Bajracharya, S., Stoffel, M., 2012. The State and Fate of Himalayan Glaciers. *Science* 336, 310–314. <https://doi.org/10.1126/science.1215828>
- Carey, M., Huggel, C., Bury, J., Portocarrero, C., Haeberli, W., 2012. An integrated socio-environmental framework for glacier hazard management and climate change adaptation: lessons from Lake 513, Cordillera Blanca, Peru. *Clim. Change* 112, 733–767. <https://doi.org/10.1007/s10584-011-0249-8>
- Carrivick, J.L., Heckmann, T., 2017. Short-term geomorphological evolution of proglacial systems. *Geomorphology, Sediment cascades in cold climate geosystems* 287, 3–28. <https://doi.org/10.1016/j.geomorph.2017.01.037>
- Carrivick, J.L., Tweed, F.S., 2016. A global assessment of the societal impacts of glacier outburst floods. *Glob. Planet. Change* 144, 1–16. <https://doi.org/10.1016/j.gloplacha.2016.07.001>
- Carrivick, J.L., Tweed, F.S., 2013. Proglacial lakes: character, behaviour and geological importance. *Quat. Sci. Rev.* 78, 34–52. <https://doi.org/10.1016/j.quascirev.2013.07.028>
- Christen, M., Kowalski, J., Bartelt, P., 2010. RAMMS: Numerical simulation of dense snow avalanches in three-dimensional terrain. *Cold Reg. Sci. Technol.* 63, 1–14. <https://doi.org/10.1016/j.coldregions.2010.04.005>



- Cook, K.L., Andermann, C., Gimbert, F., Adhikari, B.R., Hovius, N., 2018. Glacial lake outburst floods as drivers of fluvial erosion in the Himalaya. *Science* 362, 53–57. <https://doi.org/10.1126/science.aat4981>
- Cook, S.J., Quincey, D.J., 2015. Estimating the volume of Alpine glacial lakes. *Earth Surf. Dyn.* 3, 559–575. <https://doi.org/10.5194/esurf-3-559-2015>
- D. D. More, B. K. Gavit, S. B. Nandgude, 2024. Hydrologic Engineering Centers-River Analysis System (HEC-RAS) - A Review. *J. Agric. Res. Technol.* 49, 139–150. <https://doi.org/10.56228/JART.2024.49120>
- Das, S., Ramsankaran, R., 2025. In-situ bathymetry and volume estimation of four glacial lakes in western Himalaya. *J. Glaciol.* 71, e95. <https://doi.org/10.1017/jog.2025.10082>
- Dubey, S., Goyal, M.K., 2020. Glacial Lake Outburst Flood Hazard, Downstream Impact, and Risk Over the Indian Himalayas. *Water Resour. Res.* 56, e2019WR026533. <https://doi.org/10.1029/2019WR026533>
- Dubey, S., Sattar, A., Gupta, V., Goyal, M.K., Haritashya, U.K., Kargel, J.S., 2024. Transboundary hazard and downstream impact of glacial lakes in Hindu-Kush Karakoram Himalayas. *Sci. Total Environ.* 914, 169758. <https://doi.org/10.1016/j.scitotenv.2023.169758>
- Emmer, A., 2024. Infilled lakes (Pampas) of the Cordillera Blanca, Peru: Inventory, sediment storage, and paleo outbursts. *Prog. Phys. Geogr. Earth Environ.* 48, 208–230. <https://doi.org/10.1177/03091333241227799>
- Emmer, A., Cochachin, A., 2013. The causes and mechanisms of moraine-dammed lake failures in the Cordillera Blanca, North American Cordillera, and Himalayas. *AUC Geogr.* 48, 5–15. <https://doi.org/10.14712/23361980.2014.23>
- Emmer, A., Harrison, S., Mergili, M., Allen, S., Frey, H., Huggel, C., 2020. 70 years of lake evolution and glacial lake outburst floods in the Cordillera Blanca (Peru) and implications for the future. *Geomorphology* 365, 107178. <https://doi.org/10.1016/j.geomorph.2020.107178>
- Emmer, A., Vilca, O., Salazar Checa, C., Li, S., Cook, S., Pummer, E., Hrebrina, J., Haeberli, W., 2025. Causes, consequences and implications of the 2023 landslide-induced Lake Rasac glacial lake outburst flood (GLOF), Cordillera Huayhuash, Peru. *Nat. Hazards Earth Syst. Sci.* 25, 1207–1228. <https://doi.org/10.5194/nhess-25-1207-2025>
- Emmer, A., Vilímek, V., 2014. New method for assessing the susceptibility of glacial lakes to outburst floods in the Cordillera Blanca, Peru. *Hydrol. Earth Syst. Sci.* 18, 3461–3479. <https://doi.org/10.5194/hess-18-3461-2014>
- Evans, S., 1986. Landslide Damming in the Cordillera of Western Canada.
- Farinotti, D., Huss, M., Fürst, J.J., Landmann, J., Machguth, H., Maussion, F., Pandit, A., 2019. A consensus estimate for the ice thickness distribution of all glaciers on Earth. *Nat. Geosci.* 12, 168–173. <https://doi.org/10.1038/s41561-019-0300-3>
- Fischer, L., Purves, R.S., Huggel, C., Noetzli, J., Haeberli, W., 2012. On the influence of topographic, geological and cryospheric factors on rock avalanches and rockfalls in high-mountain areas. *Nat. Hazards Earth Syst. Sci.* 12, 241–254. <https://doi.org/10.5194/nhess-12-241-2012>
- Frey, H., Huggel, C., Chisolm, R.E., Baer, P., McArdell, B., Cochachin, A., Portocarrero, C., 2018. Multi-Source Glacial Lake Outburst Flood Hazard Assessment and Mapping for Huaraz, Cordillera Blanca, Peru. *Front. Earth Sci.* 6. <https://doi.org/10.3389/feart.2018.00210>
- Fujita, K., Sakai, A., Takenaka, S., Nuimura, T., Surazakov, A.B., Sawagaki, T., Yamanokuchi, T., 2013. Potential flood volume of Himalayan glacial lakes. *Nat. Hazards Earth Syst. Sci.* 13, 1827–1839. <https://doi.org/10.5194/nhess-13-1827-2013>



- Furian, W., Maussion, F., Schneider, C., 2022. Projected 21st-Century Glacial Lake Evolution in High Mountain Asia. *Front. Earth Sci.* 10. <https://doi.org/10.3389/feart.2022.821798>
- Granshaw, F.D., Fountain, A.G., 2006. Glacier change (1958–1998) in the North Cascades National Park Complex, Washington, USA. *J. Glaciol.* 52, 251–256. <https://doi.org/10.3189/172756506781828782>
- Gruber, S., 2012. Derivation and analysis of a high-resolution estimate of global permafrost zonation. *The Cryosphere* 6, 221–233. <https://doi.org/10.5194/tc-6-221-2012>
- Gruber, S., Fleiner, R., Guegan, E., Panday, P., Schmid, M.-O., Stumm, D., Wester, P., Zhang, Y., Zhao, L., 2017. Review article: Inferring permafrost and permafrost thaw in the mountains of the Hindu Kush Himalaya region. *The Cryosphere* 11, 81–99. <https://doi.org/10.5194/tc-11-81-2017>
- Gruber, S., Haeberli, W., 2007. Permafrost in steep bedrock slopes and its temperature-related destabilization following climate change. *J. Geophys. Res. Earth Surf.* 112. <https://doi.org/10.1029/2006JF000547>
- Haeberli, W., Hoelzle, M., Paul, F., Zemp, M., 2007. Integrated monitoring of mountain glaciers as key indicators of global climate change: the European Alps. *Ann. Glaciol.* 46, 150–160. <https://doi.org/10.3189/172756407782871512>
- Haeberli, W., Noetzli, J., Arenson, L., Delaloye, R., Gärtnert-Roer, I., Gruber, S., Isaksen, K., Kneisel, C., Krautblatter, M., Phillips, M., 2010. Mountain permafrost: development and challenges of a young research field. *J. Glaciol.* 56, 1043–1058. <https://doi.org/10.3189/002214311796406121>
- Haeberli, W., Schaub, Y., Huggel, C., 2017. Increasing risks related to landslides from degrading permafrost into new lakes in de-glaciating mountain ranges. *Geomorphology, Permafrost and periglacial research from coasts to mountains* 293, 405–417. <https://doi.org/10.1016/j.geomorph.2016.02.009>
- Haritashya, U.K., Kargel, J.S., Shugar, D.H., Leonard, G.J., Stratton, K., Watson, C.S., Shean, D., Harrison, S., Mandli, K.T., Regmi, D., 2018. Evolution and Controls of Large Glacial Lakes in the Nepal Himalaya. *Remote Sens.* 10, 798. <https://doi.org/10.3390/rs10050798>
- Harrison, S., Kargel, J.S., Huggel, C., Reynolds, J., Shugar, D.H., Betts, R.A., Emmer, A., Glasser, N., Haritashya, U.K., Klimeš, J., Reinhardt, L., Schaub, Y., Wiltshire, A., Regmi, D., Vilímek, V., 2018. Climate change and the global pattern of moraine-dammed glacial lake outburst floods. *The Cryosphere* 12, 1195–1209. <https://doi.org/10.5194/tc-12-1195-2018>
- Hjort, J., Streletskiy, D., Doré, G., Wu, Q., Bjella, K., Luoto, M., 2022. Impacts of permafrost degradation on infrastructure. *Nat. Rev. Earth Environ.* 3, 24–38. <https://doi.org/10.1038/s43017-021-00247-8>
- Huggel, C., Gruber, S., Caplan-Auerbach, S., Wessels, R.L., Molnia, B.F., 2008. The 2005 Mt. Steller, Alaska, rock-ice avalanche: a large slope failure in cold permafrost. Presented at the 9th International Conference on Permafrost, pp. 747–752.
- Huggel, C., Kääb, A., Haeberli, W., Teyssiere, P., Paul, F., 2002. Remote sensing based assessment of hazards from glacier lake outbursts: a case study in the Swiss Alps. *Can. Geotech. J.* 39, 316–330. <https://doi.org/10.1139/t01-099>
- Huggel, C., Scheel, M., Albrecht, F., Andres, N., Calanca, P., Jurt, C., Khabarov, N., Mira-Salama, D., Rohrer, M., Salzmann, N., Silva, Y., Silvestre, E., Vicuña, L., Zappa, M., 2015. A framework for the science contribution in climate adaptation: Experiences from science-policy processes in the Andes. *Environ. Sci. Policy* 47, 80–94. <https://doi.org/10.1016/j.envsci.2014.11.007>



- Ikeda, N., Narama, C., Gyalson, S., 2016a. Knowledge Sharing for Disaster Risk Reduction: Insights from a Glacier Lake Workshop in the Ladakh Region, Indian Himalayas. *Mt. Res. Dev.* 36, 31–40. <https://doi.org/10.1659/MRD-JOURNAL-D-15-00035.1>
- Ikeda, N., Narama, C., Gyalson, S., 2016b. Knowledge Sharing for Disaster Risk Reduction: Insights from a Glacier Lake Workshop in the Ladakh Region, Indian Himalayas. *Mt. Res. Dev.* 36, 31–40. <https://doi.org/10.1659/MRD-JOURNAL-D-15-00035.1>
- Islam, N., Carrivick, J.L., Coulthard, T., Westoby, M., Dunning, S., Gindraux, S., 2025. A growing threat of multi-hazard cascades highlighted by the Birch Glacier collapse and Blatten landslide in the Swiss Alps. *Geol. Today* 41, 200–205. <https://doi.org/10.1111/gto.12526>
- Kapitsa, V., Shahgedanova, M., Machguth, H., Severskiy, I., Medeu, A., 2017. Assessment of evolution and risks of glacier lake outbursts in the Djungarskiy Alatau, Central Asia, using Landsat imagery and glacier bed topography modelling. *Nat. Hazards Earth Syst. Sci.* 17, 1837–1856. <https://doi.org/10.5194/nhess-17-1837-2017>
- Kargel, J.S., Cogley, J.G., Leonard, G.J., Haritashya, U., Byers, A., 2011. Himalayan glaciers: The big picture is a montage. *Proc. Natl. Acad. Sci.* 108, 14709–14710. <https://doi.org/10.1073/pnas.1111663108>
- Khanal, N.R., Mool, P.K., Shrestha, A.B., Rasul, G., Ghimire, P.K., Shrestha, R.B., Joshi, S.P., 2015. A comprehensive approach and methods for glacial lake outburst flood risk assessment, with examples from Nepal and the transboundary area. *Int. J. Water Resour. Dev.* 31, 219–237. <https://doi.org/10.1080/07900627.2014.994116>
- King, O., Bhattacharya, A., Bhambri, R., Bolch, T., 2019. Glacial lakes exacerbate Himalayan glacier mass loss. *Sci. Rep.* 9, 18145. <https://doi.org/10.1038/s41598-019-53733-x>
- King, O., Dehecq, A., Quincey, D., Carrivick, J., 2018. Contrasting geometric and dynamic evolution of lake and land-terminating glaciers in the central Himalaya. *Glob. Planet. Change* 167, 46–60. <https://doi.org/10.1016/j.gloplacha.2018.05.006>
- Klimeš, J., Benešová, M., Vilímek, V., Bouška, P., Cochachin Rapre, A., 2014. The reconstruction of a glacial lake outburst flood using HEC-RAS and its significance for future hazard assessments: an example from Lake 513 in the Cordillera Blanca, Peru. *Nat. Hazards* 71, 1617–1638. <https://doi.org/10.1007/s11069-013-0968-4>
- Komori, J., Koike, T., Yamanokuchi, T., Tshering, P., 2012. Glacial Lake Outburst Events in the Bhutan Himalayas. *Glob. Environ. Res.* 16, 59–70. https://doi.org/10.57466/ger.16.1_59
- Kumar, S., Shawez, M., Ansari, T.A., Rana, H., Ghildiyal, D., 2025. The Dharali Catastrophic Disaster of 05th August 2025: A Wake-Up Call from the Kheer Ganga, NW Himalaya. *Nat. Hazards Res.* <https://doi.org/10.1016/j.nhres.2025.11.001>
- Loriaux, T., Casassa, G., 2013. Evolution of glacial lakes from the Northern Patagonia Icefield and terrestrial water storage in a sea-level rise context. *Glob. Planet. Change* 102, 33–40. <https://doi.org/10.1016/j.gloplacha.2012.12.012>
- Lützow, N., Veh, G., Korup, O., 2023. A global database of historic glacier lake outburst floods. *Earth Syst. Sci. Data* 15, 2983–3000. <https://doi.org/10.5194/essd-15-2983-2023>
- Majeed, U., Rashid, I., Sattar, A., Allen, S., Stoffel, M., Nüsser, M., Schmidt, S., 2021. Recession of Gya Glacier and the 2014 glacial lake outburst flood in the Trans-Himalayan region of Ladakh, India. *Sci. Total Environ.* 756, 144008. <https://doi.org/10.1016/j.scitotenv.2020.144008>
- Mal, S., Allen, S.K., Frey, H., Huggel, C., Dimri, A.P., 2021. Sectorwise Assessment of Glacial Lake Outburst Flood Danger in the Indian Himalayan Region. *Mt. Res. Dev.* 41, R1. <https://doi.org/10.1659/MRD-JOURNAL-D-20-00043.1>



- Maurer, J.M., Schaefer, J.M., Rupper, S., Corley, A., 2019. Acceleration of ice loss across the Himalayas over the past 40 years. *Sci. Adv.* 5, eaav7266. <https://doi.org/10.1126/sciadv.aav7266>
- Mergili, M., Fischer, J.-T., Krenn, J., Pudasaini, S.P., 2017. r.avaflow v1, an advanced open-source computational framework for the propagation and interaction of two-phase mass flows. *Geosci. Model Dev.* 10, 553–569. <https://doi.org/10.5194/gmd-10-553-2017>
- Muñoz, R., Huggel, C., Frey, H., Cochachin, A., Haeberli, W., 2020. Glacial lake depth and volume estimation based on a large bathymetric dataset from the Cordillera Blanca, Peru. *Earth Surf. Process. Landf.* 45, 1510–1527. <https://doi.org/10.1002/esp.4826>
- Nicolksy, D.J., Romanovsky, V.E., 2018. Modeling Long-Term Permafrost Degradation. *J. Geophys. Res. Earth Surf.* 123, 1756–1771. <https://doi.org/10.1029/2018JF004655>
- Nie, Y., Liu, Q., Wang, J., Zhang, Y., Sheng, Y., Liu, S., 2018. An inventory of historical glacial lake outburst floods in the Himalayas based on remote sensing observations and geomorphological analysis. *Geomorphology* 308, 91–106. <https://doi.org/10.1016/j.geomorph.2018.02.002>
- Pandey, S.J., Bhat, G.M., Puri, S., Raina, N., Singh, Y., Pandita, S.K., Verma, M., Bansal, B.K., Sutar, A., 2017. Seismotectonic study of Kishtwar region of Jammu Province using local broadband seismic data. *J. Seismol.* 21, 525–538. <https://doi.org/10.1007/s10950-016-9614-4>
- Pfeffer, W.T., Arendt, A.A., Bliss, A., Bolch, T., Cogley, J.G., Gardner, A.S., Hagen, J.-O., Hock, R., Kaser, G., Kienholz, C., 2014. The Randolph Glacier Inventory: a globally complete inventory of glaciers. *J. Glaciol.* 60, 537–552.
- Pritchard, H.D., 2019. Asia's shrinking glaciers protect large populations from drought stress. *Nature* 569, 649–654. <https://doi.org/10.1038/s41586-019-1240-1>
- Pronk, J.B., Bolch, T., King, O., Wouters, B., Benn, D.I., 2021. Contrasting surface velocities between lake- and land-terminating glaciers in the Himalayan region. *The Cryosphere* 15, 5577–5599. <https://doi.org/10.5194/tc-15-5577-2021>
- Racoviteanu, A.E., Arnaud, Y., Williams, M.W., Manley, W.F., 2015. Spatial patterns in glacier characteristics and area changes from 1962 to 2006 in the Kanchenjunga–Sikkim area, eastern Himalaya. *The Cryosphere* 9, 505–523. <https://doi.org/10.5194/tc-9-505-2015>
- Rai, S.K., Dhar, S., Mehta, P., 2025. Hydrogeochemical assessment and water quality of glacier-fed catchment of Chenab basin, Kishtwar Himalaya, Jammu and Kashmir, India. *Environ. Sci. Pollut. Res.* <https://doi.org/10.1007/s11356-025-36071-6>
- Rai, S.K., Dhar, S., Sahu, R., Kumar, A., 2024. Two Decades of Glacier and Glacial Lake Change in the Dhauladhar Mountain Range, Himachal Himalayas, India (2000–2020). *J. Indian Soc. Remote Sens.* 52, 633–644. <https://doi.org/10.1007/s12524-024-01849-7>
- Ran, Y., Li, X., Cheng, G., Che, J., Aalto, J., Karjalainen, O., Hjort, J., Luoto, M., Jin, H., Obu, J., Hori, M., Yu, Q., Chang, X., 2022. New high-resolution estimates of the permafrost thermal state and hydrothermal conditions over the Northern Hemisphere. *Earth Syst. Sci. Data* 14, 865–884. <https://doi.org/10.5194/essd-14-865-2022>
- Richardson, S.D., Reynolds, J.M., 2000. An overview of glacial hazards in the Himalayas. *Quat. Int.* 65–66, 31–47. [https://doi.org/10.1016/S1040-6182\(99\)00035-X](https://doi.org/10.1016/S1040-6182(99)00035-X)
- Rinzin, S., Dunning, S., Carr, R.J., Allen, S., Wangchuk, S., Sattar, A., 2025. Redefining dangerous glacial lakes in Bhutan by integrating hydrodynamic flood mapping and downstream exposure data. *EGUsphere* 1–35. <https://doi.org/10.5194/egusphere-2025-3206>
- Rounce, D.R., Watson, C.S., McKinney, D.C., 2017. Identification of Hazard and Risk for Glacial Lakes in the Nepal Himalaya Using Satellite Imagery from 2000–2015. *Remote Sens.* 9, 654. <https://doi.org/10.3390/rs9070654>



- Sakai, A., Chikita, K., Yamada, T., 2000. Expansion of a moraine-dammed glacial lake, Tsho Rolpa, in Rolwaling Himal, Nepal Himalaya. *Limnol. Oceanogr.* 45, 1401–1408. <https://doi.org/10.4319/lo.2000.45.6.1401>
- Sato, Y., Fujita, K., Inoue, H., Sakai, A., Karma, 2022. Land- to lake-terminating transition triggers dynamic thinning of a Bhutanese glacier. *The Cryosphere* 16, 2643–2654. <https://doi.org/10.5194/tc-16-2643-2022>
- Sattar, A., Allen, S., Mergili, M., Haeberli, W., Frey, H., Kulkarni, A.V., Haritashya, U.K., Huggel, C., Goswami, A., Ramsankaran, R., 2023. Modeling Potential Glacial Lake Outburst Flood Process Chains and Effects From Artificial Lake-Level Lowering at Gepang Gath Lake, Indian Himalaya. *J. Geophys. Res. Earth Surf.* 128, e2022JF006826. <https://doi.org/10.1029/2022JF006826>
- Sattar, A., Cook, K.L., Rai, S.K., Berthier, E., Allen, S., Rinzin, S., de Vries, M.V.W., Haeberli, W., Kushwaha, P., Shugar, D.H., Emmer, A., Haritashya, U.K., Frey, H., Rao, P., Gurudin, K.S.K., Rai, P., Rajak, R., Hossain, F., Huggel, C., Mergili, M., Azam, Mohd.F., Gascoin, S., Carrivick, J.L., Bell, L.E., Ranjan, R.K., Rashid, I., Kulkarni, Anil.V., Petley, D., Schwanghart, W., Watson, C.S., Islam, N., Gupta, M.D., Lane, S.N., Bhat, S.Y., 2025a. The Sikkim flood of October 2023: Drivers, causes, and impacts of a multihazard cascade. *Science* 387, eads2659. <https://doi.org/10.1126/science.ads2659>
- Sattar, A., Emmer, A., Lhazom, T., Rai, S.K., Azam, M.F., 2025b. Flood risk from small mountain lakes. *Commun. Earth Environ.* 6, 785. <https://doi.org/10.1038/s43247-025-02758-4>
- Sattar, A., Goswami, A., Kulkarni, A.V., 2019. Application of 1D and 2D hydrodynamic modeling to study glacial lake outburst flood (GLOF) and its impact on a hydropower station in Central Himalaya. *Nat. Hazards* 97, 535–553. <https://doi.org/10.1007/s11069-019-03657-6>
- Sattar, A., Haritashya, U.K., Kargel, J.S., Karki, A., 2022. Transition of a small Himalayan glacier lake outburst flood to a giant transborder flood and debris flow. *Sci. Rep.* 12, 12421. <https://doi.org/10.1038/s41598-022-16337-6>
- Sattar, A., Haritashya, U.K., Kargel, J.S., Leonard, G.J., Shugar, D.H., Chase, D.V., 2021. Modeling lake outburst and downstream hazard assessment of the Lower Barun Glacial Lake, Nepal Himalaya. *J. Hydrol.* 598, 126208. <https://doi.org/10.1016/j.jhydrol.2021.126208>
- Schmidt, S., Nüsser, M., Baghel, R., Dame, J., 2020. Cryosphere hazards in Ladakh: the 2014 Gya glacial lake outburst flood and its implications for risk assessment. *Nat. Hazards* 104, 2071–2095. <https://doi.org/10.1007/s11069-020-04262-8>
- Schneider, D., Huggel, C., Cochachin, A., Guillén, S., García, J., 2014. Mapping hazards from glacier lake outburst floods based on modelling of process cascades at Lake 513, Carhuaz, Peru, in: *Advances in Geosciences*. Presented at the 8th EGU Alexander von Humboldt Conference “Natural Disasters, Global Change, and the Preservation of World Heritage Sites” - 8th Alexander von Humboldt International Conference on Natural Disasters, Global Change, and the Preservation of World Heritage Sites, Cusco, Peru, 12–16 November 2012, Copernicus GmbH, pp. 145–155. <https://doi.org/10.5194/adgeo-35-145-2014>
- Schwanghart, W., Worni, R., Huggel, C., Stoffel, M., Korup, O., 2016. Uncertainty in the Himalayan energy–water nexus: estimating regional exposure to glacial lake outburst floods. *Environ. Res. Lett.* 11, 074005. <https://doi.org/10.1088/1748-9326/11/7/074005>
- Shean, D.E., Bhushan, S., Montesano, P., Rounce, D.R., Arendt, A., Osmanoglu, B., 2020. A Systematic, Regional Assessment of High Mountain Asia Glacier Mass Balance. *Front. Earth Sci.* 7. <https://doi.org/10.3389/feart.2019.00363>



- Sherpa, S.F., Smith, L.C., Wang, B., Stuurman, C., 2025. Brief Communication: Multisource Remote Sensing Detects Growing Himalayan Glacial Lake Outburst Flood Hazards. EGUsphere 1–9. <https://doi.org/10.5194/egusphere-2025-133>
- Shrestha, A.B., Eriksson, M., Mool, P., Ghimire, P., Mishra, B., Khanal, N.R., 2010. Glacial lake outburst flood risk assessment of Sun Koshi basin, Nepal. *Geomat. Nat. Hazards Risk* 1, 157–169. <https://doi.org/10.1080/19475701003668968>
- Shrestha, F., Steiner, J.F., Shrestha, R., Dhungel, Y., Joshi, S.P., Inglis, S., Ashraf, A., Wali, S., Walizada, K.M., Zhang, T., 2023. A comprehensive and version-controlled database of glacial lake outburst floods in High Mountain Asia. *Earth Syst. Sci. Data* 15, 3941–3961. <https://doi.org/10.5194/essd-15-3941-2023>
- Shugar, D.H., Burr, A., Haritashya, U.K., Kargel, J.S., Watson, C.S., Kennedy, M.C., Bevington, A.R., Betts, R.A., Harrison, S., Stratton, K., 2020. Rapid worldwide growth of glacial lakes since 1990. *Nat. Clim. Change* 10, 939–945. <https://doi.org/10.1038/s41558-020-0855-4>
- Shugar, D.H., Jacquemart, M., Shean, D., Bhushan, S., Upadhyay, K., Sattar, A., Schwanghart, W., McBride, S., de Vries, M.V.W., Mergili, M., Emmer, A., Deschamps-Berger, C., McDonnell, M., Bhambri, R., Allen, S., Berthier, E., Carrivick, J.L., Clague, J.J., Dokukin, M., Dunning, S.A., Frey, H., Gascoin, S., Haritashya, U.K., Huggel, C., Kääb, A., Kargel, J.S., Kavanaugh, J.L., Lacroix, P., Petley, D., Rupper, S., Azam, M.F., Cook, S.J., Dimri, A.P., Eriksson, M., Farinotti, D., Fiddes, J., Gnyawali, K.R., Harrison, S., Jha, M., Koppes, M., Kumar, A., Leinss, S., Majeed, U., Mal, S., Muhuri, A., Noetzli, J., Paul, F., Rashid, I., Sain, K., Steiner, J., Ugalde, F., Watson, C.S., Westoby, M.J., 2021. A massive rock and ice avalanche caused the 2021 disaster at Chamoli, Indian Himalaya. *Science* 373, 300–306. <https://doi.org/10.1126/science.abb4455>
- Somos-Valenzuela, M.A., Chisolm, R.E., Rivas, D.S., Portocarrero, C., McKinney, D.C., 2016. Modeling a glacial lake outburst flood process chain: the case of Lake Palcacocha and Huaraz, Peru. *Hydrol. Earth Syst. Sci.* 20, 2519–2543. <https://doi.org/10.5194/hess-20-2519-2016>
- Stoffel, M., Allen, S.K., Ballesteros-Cánovas, J.A., Jakob, M., Oakley, N., 2024. Climate Change Effects on Debris Flows, in: Jakob, M., McDougall, S., Santi, P. (Eds.), *Advances in Debris-Flow Science and Practice*. Springer International Publishing, Cham, pp. 273–308. https://doi.org/10.1007/978-3-031-48691-3_10
- Taylor, C., Robinson, T.R., Dunning, S., Rachel Carr, J., Westoby, M., 2023. Glacial lake outburst floods threaten millions globally. *Nat. Commun.* 14, 487. <https://doi.org/10.1038/s41467-023-36033-x>
- Veh, G., Korup, O., von Specht, S., Roessner, S., Walz, A., 2019. Unchanged frequency of moraine-dammed glacial lake outburst floods in the Himalaya. *Nat. Clim. Change* 9, 379–383. <https://doi.org/10.1038/s41558-019-0437-5>
- Veh, G., Korup, O., Walz, A., 2020. Hazard from Himalayan glacier lake outburst floods. *Proc. Natl. Acad. Sci.* 117, 907–912. <https://doi.org/10.1073/pnas.1914898117>
- Veh, G., Lützow, N., Kharlamova, V., Petrakov, D., Hugonnet, R., Korup, O., 2022. Trends, Breaks, and Biases in the Frequency of Reported Glacier Lake Outburst Floods. *Earth's Future* 10, e2021EF002426. <https://doi.org/10.1029/2021EF002426>
- Veh, G., Wang, B.G., Zirzow, A., Schmidt, C., Lützow, N., Steppat, F., Zhang, G., Vogel, K., Geertsema, M., Clague, J.J., Korup, O., 2025. Progressively smaller glacier lake outburst floods despite worldwide growth in lake area. *Nat. Water* 3, 271–283. <https://doi.org/10.1038/s44221-025-00388-w>
- Wang, W., Gao, Y., Iribarren Anacona, P., Lei, Y., Xiang, Y., Zhang, G., Li, S., Lu, A., 2018. Integrated hazard assessment of Cirenmaco glacial lake in Zhangzangbo valley, Central



- Himalayas. *Geomorphology* 306, 292–305.
<https://doi.org/10.1016/j.geomorph.2015.08.013>
- Wang, W., Xiang, Y., Gao, Y., Lu, A., Yao, T., 2015. Rapid expansion of glacial lakes caused by climate and glacier retreat in the Central Himalayas. *Hydrol. Process.* 29, 859–874. <https://doi.org/10.1002/hyp.10199>
- Wang, X., Liu, S., Ding, Y., Guo, W., Jiang, Z., Lin, J., Han, Y., 2012. An approach for estimating the breach probabilities of moraine-dammed lakes in the Chinese Himalayas using remote-sensing data. *Nat. Hazards Earth Syst. Sci.* 12, 3109–3122. <https://doi.org/10.5194/nhess-12-3109-2012>
- Watson, C.S., Kargel, J.S., Shugar, D.H., Haritashya, U.K., Schiassi, E., Furfarò, R., 2020. Mass Loss From Calving in Himalayan Proglacial Lakes. *Front. Earth Sci.* 7. <https://doi.org/10.3389/feart.2019.00342>
- Westoby, M.J., Glasser, N.F., Brasington, J., Hambrey, M.J., Quincey, D.J., Reynolds, J.M., 2014. Modelling outburst floods from moraine-dammed glacial lakes. *Earth-Sci. Rev.* 134, 137–159. <https://doi.org/10.1016/j.earscirev.2014.03.009>
- Wiltshire, A.J., 2014. Climate change implications for the glaciers of the Hindu Kush, Karakoram and Himalayan region. *The Cryosphere* 8, 941–958. <https://doi.org/10.5194/tc-8-941-2014>
- Worni, R., Huggel, C., Clague, J.J., Schaub, Y., Stoffel, M., 2014. Coupling glacial lake impact, dam breach, and flood processes: A modeling perspective. *Geomorphology* 224, 161–176. <https://doi.org/10.1016/j.geomorph.2014.06.031>
- Worni, R., Huggel, C., Stoffel, M., 2013. Glacial lakes in the Indian Himalayas — From an area-wide glacial lake inventory to on-site and modeling based risk assessment of critical glacial lakes. *Sci. Total Environ.*, Changing water resources availability in Northern India with respect to Himalayan glacier retreat and changing monsoon patterns: consequences and adaptation 468–469, S71–S84. <https://doi.org/10.1016/j.scitotenv.2012.11.043>
- Yang, D., Qiu, H., Quevedo, R.P., Liu, Y., Glade, T., 2025. Birchgletscher rock-ice avalanche burying the village of Blatten on 28 May 2025, Valais, Switzerland. *Landslides*. <https://doi.org/10.1007/s10346-025-02656-y>
- Yang, L., Lu, Z., Zhao, C., Zhang, Q., Hu, X., Wang, B., 2025. Triggering factors and flooding processes of glacial lake outburst flood at Ranzerio lake. *Npj Nat. Hazards* 2, 90. <https://doi.org/10.1038/s44304-025-00147-7>
- Yanites, B.J., Clark, M.K., Roering, J.J., West, A.J., Zekkos, D., Baldwin, J.W., Cerovski-Darriau, C., Gallen, S.F., Horton, D.E., Kirby, E., Leshchinsky, B.A., Mason, H.B., Moon, S., Barnhart, K.R., Booth, A., Czuba, J.A., McCoy, S., McGuire, L., Pfeiffer, A., Pierce, J., 2025. Cascading land surface hazards as a nexus in the Earth system. *Science* 388, eadp9559. <https://doi.org/10.1126/science.adp9559>
- Zhang, G., Bolch, T., Yao, T., Rounce, D.R., Chen, W., Veh, G., King, O., Allen, S.K., Wang, M., Wang, W., 2023. Underestimated mass loss from lake-terminating glaciers in the greater Himalaya. *Nat. Geosci.* 16, 333–338. <https://doi.org/10.1038/s41561-023-01150-1>
- Zhang, J.-Y., Yang, X.-G., Fan, G., Li, H.-B., Hu, Y.-X., Zhou, J.-W., 2025. Hydraulic characteristics and geomorphic effects of the 2018 Baige landslide lake outburst flood: A reach-scale study of the mainstem over hundreds of kilometers. *CATENA* 257, 109136. <https://doi.org/10.1016/j.catena.2025.109136>
- Zhang, T., Wang, W., An, B., 2025. A massive lateral moraine collapse triggered the 2023 South Lhonak Lake outburst flood, Sikkim Himalayas. *Landslides* 22, 299–311. <https://doi.org/10.1007/s10346-024-02358-x>



- Zhang, T., Yin, Y., Li, B., Liu, X., Wang, M., Gao, Y., Wan, J., Gnyawali, K.R., 2023. Characteristics and dynamic analysis of the February 2021 long-runout disaster chain triggered by massive rock and ice avalanche at Chamoli, Indian Himalaya. *J. Rock Mech. Geotech. Eng.* 15, 296–308. <https://doi.org/10.1016/j.jrmge.2022.04.003>
- Zheng, G., Bao, A., Allen, S., Antonio Ballesteros-Cánovas, J., Yuan, Y., Jiapaer, G., Stoffel, M., 2021a. Numerous unreported glacial lake outburst floods in the Third Pole revealed by high-resolution satellite data and geomorphological evidence. *Sci. Bull.* 66, 1270–1273. <https://doi.org/10.1016/j.scib.2021.01.014>
- Zheng, G., Mergili, M., Emmer, A., Allen, S., Bao, A., Guo, H., Stoffel, M., 2021b. The 2020 glacial lake outburst flood at Jinwuco, Tibet: causes, impacts, and implications for hazard and risk assessment. *The Cryosphere* 15, 3159–3180. <https://doi.org/10.5194/tc-15-3159-2021>